Article

Biochar Derived from Water Hyacinth Biomass Chemically Activated for Dye Removal in Aqueous Solution

Marcelo Teixeira Carneiro [1,2], Alan Ícaro Sousa Morais [2], André Luiz Ferreira de Carvalho Melo [1,2], Francisco José Lustosa Ferreira [1,2], Francisco Eroni Paz Santos [2], Bartolomeu Cruz Viana [2], Josy Anteveli Osajima [2], Roosevelt D. S. Bezerra [3], Maria Del Mar Orta Cuevas [4], Ramón Raudel Peña-Garcia [5], Luciano C. Almeida [5] and Edson C. Silva-Filho [2,*]

1   Federal Institute of Piauí, Campus Floriano, Floriano 64800-000, PI, Brazil; marcelo.teixeira@ifpi.edu.br (M.T.C.); andreluiz@ifpi.edu.br (A.L.F.d.C.M.); franciscojufpi@gmail.com (F.J.L.F.)
2   Interdisciplinary Laboratory for Advanced Materials, Federal University of Piauí, Teresina 64049-550, PI, Brazil; alanicaro@gmail.com (A.Í.S.M.); franciscoeroni@gmail.com (F.E.P.S.); bartolomeu@ufpi.edu.br (B.C.V.); josyosajima@ufpi.edu.br (J.A.O.)
3   Federal Institute of Piauí, Teresina-Central Campus, Teresina 64000-060, PI, Brazil; rooseveltdsb@ifpi.edu.br
4   Departamento de Química Analítica, Facultad de Farmacia, Universidad de Sevilla, 41012 Sevilla, Spain; enmaorta@us.es
5   Academic Unit of Cabo de Santo Agostinho, Rural Federal University of Pernambuco, Cabo de Santo Agostinho 54518-430, PE, Brazil; rraudelp@gmail.com (R.R.P.-G.); luciano.calmeida@ufpe.br (L.C.A.)
*   Correspondence: edsonfilho@ufpi.edu.br

Abstract: Rapid industrial development has led to the use of numerous dyes responsible for significant water pollution worldwide. Adsorbents have been developed to treat these waters, mainly in the form of activated biochar, which has several advantages, one of which is its good surface characteristics, such as high surface area and pore volume. The objective of the investigation was to analyze the efficiency of removing the methylene blue model dye in aqueous solutions through the adsorption process using biochar chemically activated from the leaf and stem of water hyacinth (*Eichhornio crassipes*) as a bioadsorbent. This study carbonized the stem and leaf containing zinc chloride at 600 °C. The materials were characterized by different techniques and were tested for their ability to adsorb methylene blue. The activated stem and leaf biochars removed approximately 285.71 and 322.58 mg g^{-1} of the dye, respectively, indicating that the adsorption is more significant in the leaf. Pseudo-second-order kinetics was the most suitable model to describe dye adsorption on biochars, and the experimental isotherm data fit the Langmuir model. It is concluded that the application of activated water hyacinth biochar is a renewable resource with the potential for effluent treatment.

Keywords: *Eichhornia crassipes*; biochar; activation; methylene blue

1. Introduction

Drinking water resources worldwide are minimal, and climate change increasingly affects available supplies [1], in addition to the rapid industrial development employing numerous dyes responsible for the significant pollution of rivers and other bodies of water [2,3]. These two factors have led the world to various environmental problems, which can destroy plant life [4] and harm aquatic organisms and humans [5].

Dyes are used in various industries, such as textiles, paper, leather dyeing, cosmetics, food, and other industries. They are known to be toxic and persistent in the environment and require physicochemical techniques to degrade them [6]. Most dyes have carcinogenic, teratogenic, and mutagenic effects. Therefore, managing dyes in wastewater is a complex but crucial issue [7,8].

Methylene blue is among the most common contaminant dyes in wastewater [9] as it is widely used as a synthetic dye for textiles [10], in the coloring of silk, wool, and cotton, among other fabrics [11], as well as in the pharmaceutical industry [12]. Therefore, it is necessary to remove it from industrial discharge [3]. Developing appropriate techniques to remove methylene blue from effluents is essential to preserve the natural environment and human health [13]. Adsorption is an effective process for removing dyes from contaminated water [14]. It has many advantages, such as high adaptability [15], simplicity of design, economic viability, high efficiency, and an environmentally benign nature [16]. In recent years, much attention has been paid to the design and synthesis of new-generation adsorbents to improve adsorption capacity, cost-effectiveness, and recyclability and reduce energy consumption for practical applications [7].

Attempts to use natural biomass as an organic substitute in hybrid assemblies (instead of synthetic polymers) are still incipient. Research must be developed to expand the advancement of science in this field [17]. Several naturally available supports, especially vegetable bioadsorbents, still have much potential for developing investigations [18]. Due to the characteristics of renewability, economy, and natural porous structure, in addition to considering solid waste [19], various bioadsorbents have been used, including straw [7], fruit peel [16], pseudostem fibers [20], and sugarcane bagasse of sugarcane [21], among others, showing promise for their application in the treatment of polluted effluents.

Bioadsorbents have been used extensively in activated biochar and have good surface characteristics, such as a high surface area and pore volume. Furthermore, activated biochar may contain functional groups that interact with contaminating molecules. These characteristics make it a good material for adsorption operations with a high capacity for removing contaminants.

Regarding the production of activated biochar, there is great interest in research focusing on alternatives and low-cost precursor materials [22]. Among these materials that can be used to produce bioadsorbents in the form of activated biochar, water hyacinth (Scientific name: *Eichhornia crassipes*) stands out, which is suitable for removing contaminants in aquatic environments. Furthermore, it is crucial to highlight that this plant presents a significant proliferation in eutrophic aquatic environments. It is widely recognized on a global scale as an invasive species that threatens the survival of aquatic organisms as it obstructs the entry of sunlight, thereby depriving aquatic life of essential environmental resources, including atmospheric oxygen [23]. However, it is considered one of the most complex invasive species in aquatic ecosystems [24], whose dense mat makes water navigation, irrigation, fishing with power generation, and recreational activities complex [25]. Furthermore, the large dimensions of the water hyacinth, which can reach up to a meter, block sunlight, depriving aquatic life of environmental resources such as atmospheric oxygen [26].

The methods of removing these plants in aquatic environments include mechanical extraction and disposal on land, which is also a problem [23]. However, it becomes more advantageous than herbicide control, which introduces secondary water pollution into water bodies through chemical contamination [26]. Disposing of its biomass is still challenging due to the cost incurred in its removal and disposal. Furthermore, the spread of this floating perennial plant in different countries on all continents has generated global concern [23].

The water hyacinth residue can be considered for synthesizing new adsorbents to remove environmental contaminants and add commercial value to the product [26]. Although previous studies have shown the use of activated biochar produced from water hyacinth, most have focused on waste from the pharmaceutical industry, such as naproxen [27], fluoroquinolones [28], 2,4,6-trichlorophenol [27,29], and nuclear engineering—Uranium VI [30]. Another study involved the evaluation of this biochar for the adsorption of Remazol Brilliant Red 3BS (RBR 3BS) [31]. However, the literature has not identified reports on using water hyacinth as activated carbon with zinc chloride ($ZnCl_2$) to remove methylene blue dye.

Considering that water hyacinth is an aquatic plant of growing interest in wastewater management [32], as it is a renewable, cheap, and widely available material in nature, with the potential to adsorb pollutants with mutagenic and carcinogenic properties, including synthetic dyes [33], the development of this study is justified. The novelty of this work is the use of water hyacinth in producing biochar activated with $ZnCl_2$ and its use as a bioadsorbent. Therefore, this study aimed to analyze the removal of the methylene blue model dye in aqueous solutions through the adsorption process using chemically activated water hyacinth (*Eichhornia crassipes*) biochar as a bioadsorbent.

2. Materials and Methods

2.1. Materials and Reagents

The water hyacinths (Scientific name: *Eichhornia crassipes*) were collected from the Matias de Augusto Oliveira Matos environment park in Teresina (PI). The water hyacinths are registered in SisGen number ABD61DA. Reagents used in the adsorption experiments were methylene blue ($C_{16}H_{18}SN_3Cl$, Dinâmica—Cabedelo, Brazil), hydrochloric acid (HCl, Dinâmica, 38%—Brazil), sodium hydroxide (NaOH, Dinâmica, 98%, Brazil), sodium chloride sodium (NaCl, Dinâmica, 99%, Brazil), zinc chloride ($ZnCl_2$, Dinâmica, 97%, Brazil), and distilled water. All reagents were of analytical grade, and no prior purification was required.

2.2. Preparation of Activated Biochars

After collecting the water hyacinth, the roots were removed and discarded, and the rest of the plants were washed in running water and left in the sun to dry for three days in an open place to reduce humidity. Then, the stems and leaves were separated and placed in an oven at 50 °C for 24 h [34]. After drying, the stem and leaf were crushed and passed through a 425 μm granulometric sieve.

To produce activated stem and leaf biochars, $ZnCl_2$ was introduced into the biomasses in a 1:2 ratio (adsorbent mass per zinc chloride mass) in aqueous solution for 24 h on a shaker table with rotation 120 rpm at a temperature of 25 °C [35]. Subsequently, the materials were filtered and placed in an oven at 100 °C to remove the remaining moisture [36]. The hyacinth water from the stem and leaf samples containing $ZnCl_2$ was then subjected to carbonization at 600 °C for 1 h in the muffle, model CE–800/S–4, to remove volatile materials [37,38]. After removing from the muffle, the activated biochars were washed with hydrochloric acid (2%) to eliminate excess zinc chloride and distilled water until the pH was neutral [39]. Finally, the samples were dried again at 100 °C. The materials obtained are now called activated biochar from the leaf of the water hyacinth (LAB) and activated biochar from the stem of the water hyacinth (SAB).

2.3. Biochars Characterization

XRD measurements were used from activated biochars. Analysis was carried out on an X-ray diffractometer (Labx-XRD 600, Shimadzu, Kyoto, Japan), using Kα-Cu radiation = 1.5418, in a range of 2 θ (3–75°), a voltage of 40 kV, and the current of 30 mA.

Fourier transform infrared spectroscopy was used to obtain the functional groups in the activated biochars. The spectra were determined using a Bruker (Billerica, MA, USA) spectrophotometer, model Vertex 70, in the ATR (attenuated total reflectance) configuration. The spectra were found with 60 scans in the 600 to 4000 cm^{-1} range.

Scanning electron microscopy (SEM) was performed using SEM Tescan® Vega3® LMU® equipment (Männedorf, Switzerland). A voltage acceleration of 30 kV was used, using the images to define the shape and surface properties of the adsorbents.

Thermogravimetric curves were obtained using a thermal analyzer (Shimadzu, DT-60). A 25 to 1000 °C temperature range was established at a heating rate of 10 °C/min in an inert nitrogen atmosphere.

Raman analysis was performed on activated biochar samples using a Raman spectrometer (Horiba-Jobin-Yvon, LabRam HR Evolution, Bensheim, Germany). Raman spectra

were obtained using an excitation wavelength of 785 nm, a laser beam power of 1%, an exposure time of 30 s at ten different points, and a lens magnification of 50×. The curve fitting program obtained parameters including peak position, peak intensity, and peak FWHM (full width at half maximum) with the Lorentz and Gauss function. Raman spectroscopy was performed to assess better the structure and degree of graphitization of the biochars.

The surface area of the biochars was determined using the Brunauer–Emmett–Teller (BET) adsorption method [40]. The analysis was performed using ANOVA 1000e model equipment from Quantachrome Autosorb-iQ Instruments (Boynton Beach, FL, USA). Initially, the sample was weighed in a specific sample container (200 mg). The sample was subjected to degassing treatment (removing impurities and/or adsorbing water at 80 °C for 6 h). Finally, the texture properties of the materials were determined from the result of nitrogen (N_2) adsorption/desorption isotherms at 77 K. Thus, the surface area, pore volume, and average pore diameter were calculated.

2.4. Zero Charge Point (pH_{pzc})

The point of zero charge (pH_{pzc}) methodology refers to a point at which the surface charge of the adsorbent is neutral [41]. Samples of 20.00 mg of LAB or SAB were added to 20.00 mL of NaCl (0.1 mol L^{-1}), where the pH of the solution was adjusted in the range of 2 to 11 [42].

The pH was adjusted using NaOH solutions (1.0 mol L^{-1} and 0.1 mol L^{-1}) and HCl solutions (1.0 mol L^{-1} and 0.1 mol L^{-1}). The pH reading was performed on a pH meter (pH meter model PHS-3E—EVEN) [43]. The mixtures were stirred at 140 rpm for 24 h at 25 °C, followed by pH measurement. The pH before and after stirring was marked as pH_0 and pH_f, respectively. The delta pH was determined from Equation (1) [44].

$$\Delta pH = pH_0 - pH_f \tag{1}$$

2.5. Influence of pH

Dye solutions were prepared at pH 4, 7, and 10, where the pH was adjusted with HCl/NaOH solutions (0.1 mol L^{-1}) to verify the influence of pH on the adsorption process. The concentration of 700.00 mg L^{-1} of the dye was kept, and the study was carried out in triplicate at a temperature of 25 °C [43,45]. Then, 50.00 mg samples of activated biochars were placed in contact with 20.00 mL of methylene blue dye solution (MB) under constant agitation for 24 h at a concentration of 700.00 mg L^{-1}. After, the solutions were centrifuged and diluted. Concentrations were determined in a UV-Vis spectrophotometer (Agilent Technologies—Cary 60, Santa Clara, CA, USA) using a pre-established calibration curve at a wavelength of 663 nm, referring to the MB dye. The result of the adsorbed amount was calculated using Equation (2) [43].

$$q_e = \frac{\left(C_i - C_f\right)}{m} V \tag{2}$$

where C_i and C_f represent the initial and final concentrations (mg L^{-1}) of the dye, respectively; m corresponds to the mass of the adsorbent in grams; and V equals the volume in liters of the dye solution used.

2.6. Adsorption Kinetics

Kinetics was used to describe the control steps of the adsorption process and the equilibrium time [46]. Kinetic studies of SAB and LAB were developed at optimal pH (where the best adsorption occurred). The procedures used were similar to the results obtained in the previous section. Initially, 50.00 mg of activated stem and leaf biochars were placed in contact with 20.00 mL of MB solutions with constant stirring at 140 rpm for 4 h. The tests were conducted in triplicate at 25 °C [43].

The aliquots were centrifuged and determined on a UV-vis spectrophotometer using the pre-established calibration curve. The pseudo-first and second orders represented the kinetics obtained, expressed in Equations (3) and (4), respectively [47,48].

$$\ln\left(q_e - q_t\right) = \ln q_e - k_1 \cdot t \tag{3}$$

$$\frac{t}{q_t} = \frac{1}{k_2 \cdot q_e^2} + \frac{t}{q_e} \tag{4}$$

where q_e and q_t are the amounts of adsorbed dye (mg g^{-1}) at equilibrium and at time t, respectively; k_1 represents the adsorption constant of the pseudo-first-order model (min^{-1}), and k_2 is the pseudo-second-order kinetic model (mg g^{-1} min^{-1}).

2.7. Adsorption Isotherms

The isotherms were evaluated from the equilibrium adsorption constants, which mathematical models can determine. Furthermore, isothermal models indicate an idea of the adsorption capacity of an adsorbent [49]. The test was carried out in triplicate at 25 °C, with an optimal pH (where the best adsorption occurred). Then, 50.00 mg of SAB and LAB were weighed and placed in Erlenmeyer with 20.00 mL of MB solution, varying the concentrations between 550.00 and 1450.00 mg L^{-1}, stirred at the best equilibrium time found in the kinetic experiment [50].

The adsorption data in the present study were modeled by Freundlich and Langmuir models, which are widely used to describe the amount of relationship between adsorbed and the equilibrium concentration [23,51]. The Freundlich isotherm is used to study the multilayer coverage of adsorbate on a heterogeneous surface [52]. The Langmuir isotherm is used to characterize the monolayer cover [53]. These models are presented in the following equations:

Equation (5) has the linearized form of the Freundlich equation:

$$\ln q_e = \ln K_F + \frac{1}{n}\ln C_e \tag{5}$$

where K_F is the Freundlich adsorption constant related to the adsorption capacity, $1/n$ is the constant related to the surface heterogeneity, which represents the amount of adsorbed species per mass of the bioadsorbent (mg g^{-1}), and C_e represents the equilibrium concentration of the adsorbate (mg L^{-1}) [54].

Equation (6) expresses the linearized form of the Langmuir equation:

$$\frac{C_e}{q_e} = \frac{1}{q_{max}} \cdot C_e + \frac{1}{K_L \cdot q_{max}} \tag{6}$$

where q_e is the amount of adsorbed species per mass of the bioadsorbent (mg g^{-1}), q_{max} is the maximum amount of adsorbed species per mass of the bioadsorbent (mg g^{-1}), C_e represents the equilibrium concentration of the adsorbate (mg L^{-1}), and K_L is the Langmuir adsorption constant related to the chemical equilibrium between the adsorbate and the adsorbent (mg L^{-1}) [55].

3. Results and Discussion

3.1. Characterization of Adsorbents

Figure 1 shows the results of the XRD and FTIR of the activated biochars under study. Figure 1a presents the XRD of the LAB (1a1) and SAB (1a2). It is possible to observe the absence of sharp diffraction peaks [56], showing only broad peaks in the 2 θ region between 20 and 30° for both biochars, suggesting the existence of a graphitic carbon stain, which can be formed during the decomposition of the material [57], confirming an amorphous structure [58], typical of activated biochars [59]. XRD showed that the structures of the biochars are compatible with other biochars already described, which were favorable for

use as adsorbents [60]. Corroborating these results, Cao et al. [61] observed by XRD, in multiporous activated biochars derived from recyclable long-rooted water hyacinths, only one broad peak with a maximum at 24.4°, also indicating a graphic carbon stain and the formation of carbons with low crystallinity.
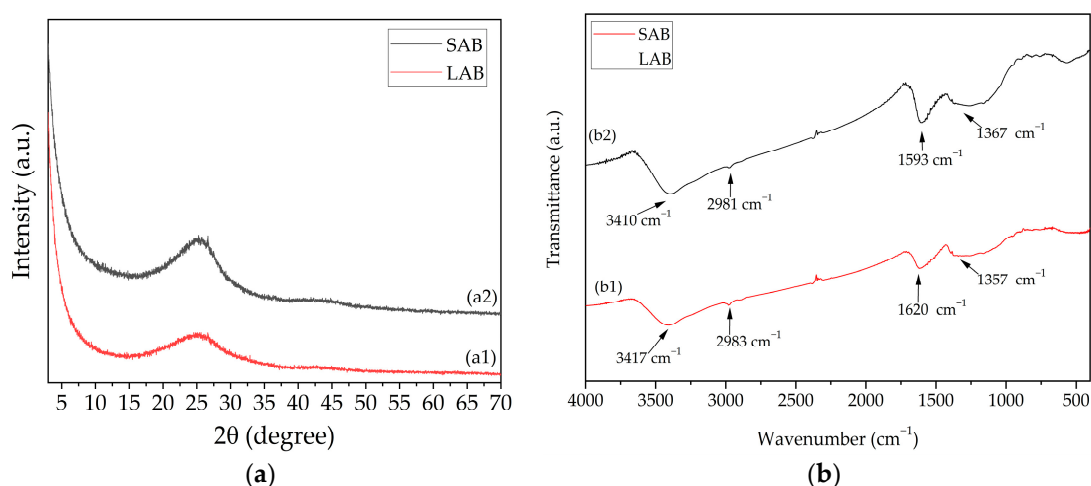
**Figure 1.** (**a**) X-ray diffractogram patterns of activated biochars: (**a1**) LAB and (**a2**) SAB; (**b**) FTIR spectra: (**b1**) LAB and (**b2**) SAB.

The FTIR spectra of LAB and SAB are found in Figure 1b, where it is possible to observe a few bands, suggesting the existence of a limited variety of surface groups. Figure 1(b1,b2) shows that the materials have similar spectra in the 3400 cm^{-1}, 3000 cm^{-1}, 1600 cm^{-1}, and 1400 cm^{-1} ranges. In the 3400 cm^{-1} range, the bands refer to stretching vibrations (OH), data that confirm the existence of hydroxylated groups on the surface [28]. The bands observed between 3000 and 2900 cm^{-1} can be attributed to methylene groups (CH) and (CH_2) [62]. Between 1620 and 1590 cm^{-1} refers to the bond stretch (C=C) of aromatic groups of the biochar structure [31]. In the 1357 cm^{-1} bands, the presence of C=O groups was verified [63].

In Figure 2, the morphological structures of the LAB (Figure 2a,b) and SAB (Figure 2c,d) are also presented under different magnifications, explaining the shape and surface properties of the adsorbent. The LAB and SAB have structures with many irregular, rough, and porous cavities [64]. These cavities were generated during the carbonization process due to chemical activation with $ZnCl_2$ [65], which may facilitate the dye penetration into the biochar pores of the product [66]. The micrograph confirms that the LAB and SAB have a porous nature and fundamental and desired characteristics in an adsorbent [67], making them potent biochar in adsorption applications [65]. Although the LAB and SAB have the same structure, they are separate studies since morphology and porosity can influence adsorption capacity [67].

TG and DTG analyses of the LAB and SAB are shown in Figure 3(a1–a4). The TG and DTG data from the LAB (Figure 3(a1,a3)) show three stages. The first stage occurs around 41 °C; the second, between temperatures of 600 and 750 °C; and the third stage is above 900 °C, with results that indicate similarity to the SAB.

In the TG and DTG (Figure 3(a2,a4)), it is possible to verify that the thermal profile of the SAB can be divided into three stages, similar to the LAB material. The first stage reaches a maximum temperature of approximately 52 °C and is related to water evaporation [59]. The second stage occurs at a temperature of 684 °C and is due to the opening of new pores through cell wall degradation [68]. The third and final step occurs above 900 °C and is associated with the combustion of fixed carbon in the sample [1].
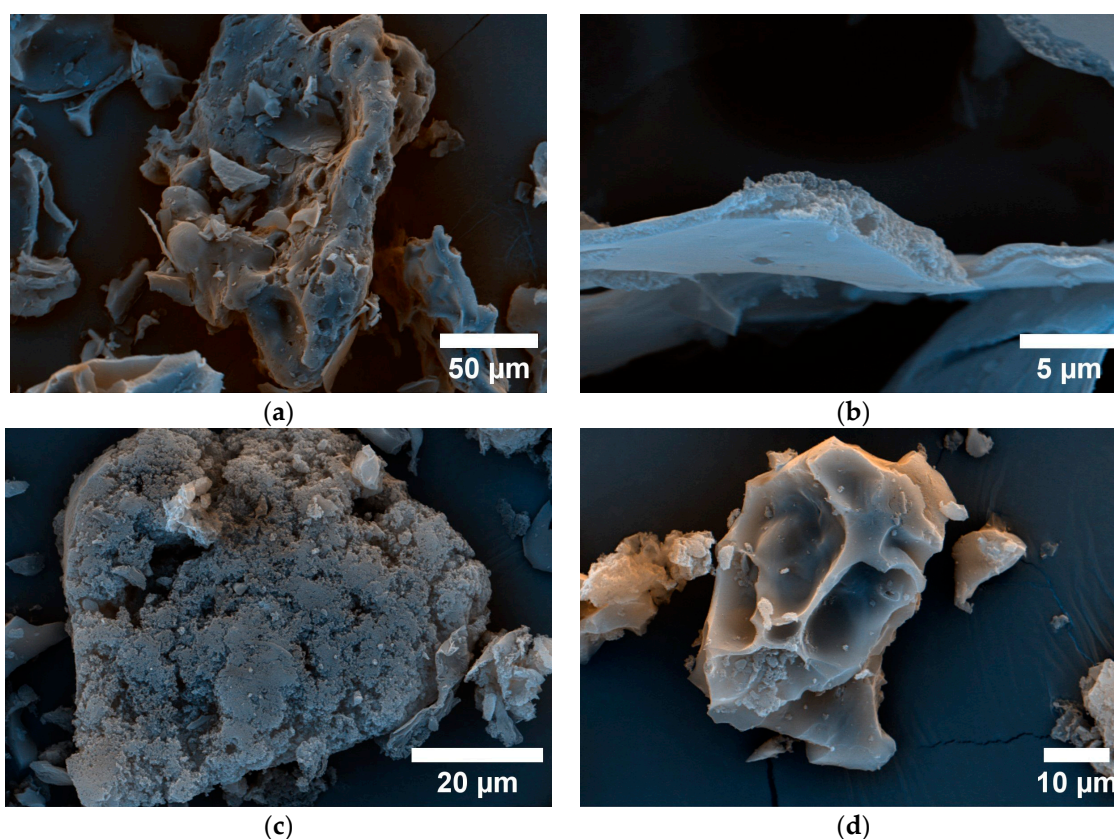
Figure 2. SEM—activated biochar micrograph of the part of the leaf of the water hyacinth (LAB) and the part of the stem of the water hyacinth (SAB): (**a**,**b**) LAB, (**c**,**d**) SAB.

Observing the residual mass of the LAB and SAB above 900 °C (Figure 3(a1,a2)), the LAB had a higher residual content than the SAB, with 64% and 70%, respectively. It is therefore evident that the mass loss was slight, which indicates the activation of the biochar, approximately, at this temperature [69].

This higher amount of residues produced after SAB pyrolysis in the LAB is because water hyacinth has a higher proportion of lignin (10.88%) compared to leaf (8.36%), as well as cellulose (27.79% for the stem and 20.81% for the leaf) and hemicellulose (30.24% for the stem and 29.71% for the leaf) [70]. Such characteristics indicate that the leaf can biodegrade faster than the stem [70].

Figure 3b shows the ΔpH values of the activated biochars, where the points that intersect ΔpH = 0 correspond to pH_{pzc}. The pH_{pzc} values found were approximately 5.1 and 6.4 for the LAB (Figure 3(b1)) and SAB (Figure 3(b2)), respectively. The surface charge is positive for pH values below pH_{pzc}, suggesting favored anionic species adsorption [71]. On the contrary, for values above pH_{pzc}, the activated biochar surface is negatively charged, showing favorable cationic dye adsorption [72]. The electrostatic attraction between MB molecules and activated biochar will be stronger at a higher pH [73].

Such results are close to the estimated pH_{pzc} values of the leaf and stem samples of natural water hyacinth, identified as 7.6 and 7.4, respectively. As mentioned for biochars, for pH values below pH_{pzc}, the surface charge is positive, indicating the adsorption of anionic species, while values above pH_{pzc} favor the adsorption of cationic species [70].

The Raman spectra of the LAB and SAB can be found in Figure 3c,d. Biochars show two typical carbon bands for both [74]. The D_1 band at 1350 cm^{-1} represents stretching vibrations of sp^3 carbons (i.e., related to defects in the carbon structure) [75]. The G band at 1580 cm^{-1} shows sp carbon stretching vibrations (associated with less defective and more ordered graphitic carbon atoms) [76].

(a)

(b)

(c)

(d)

(e)
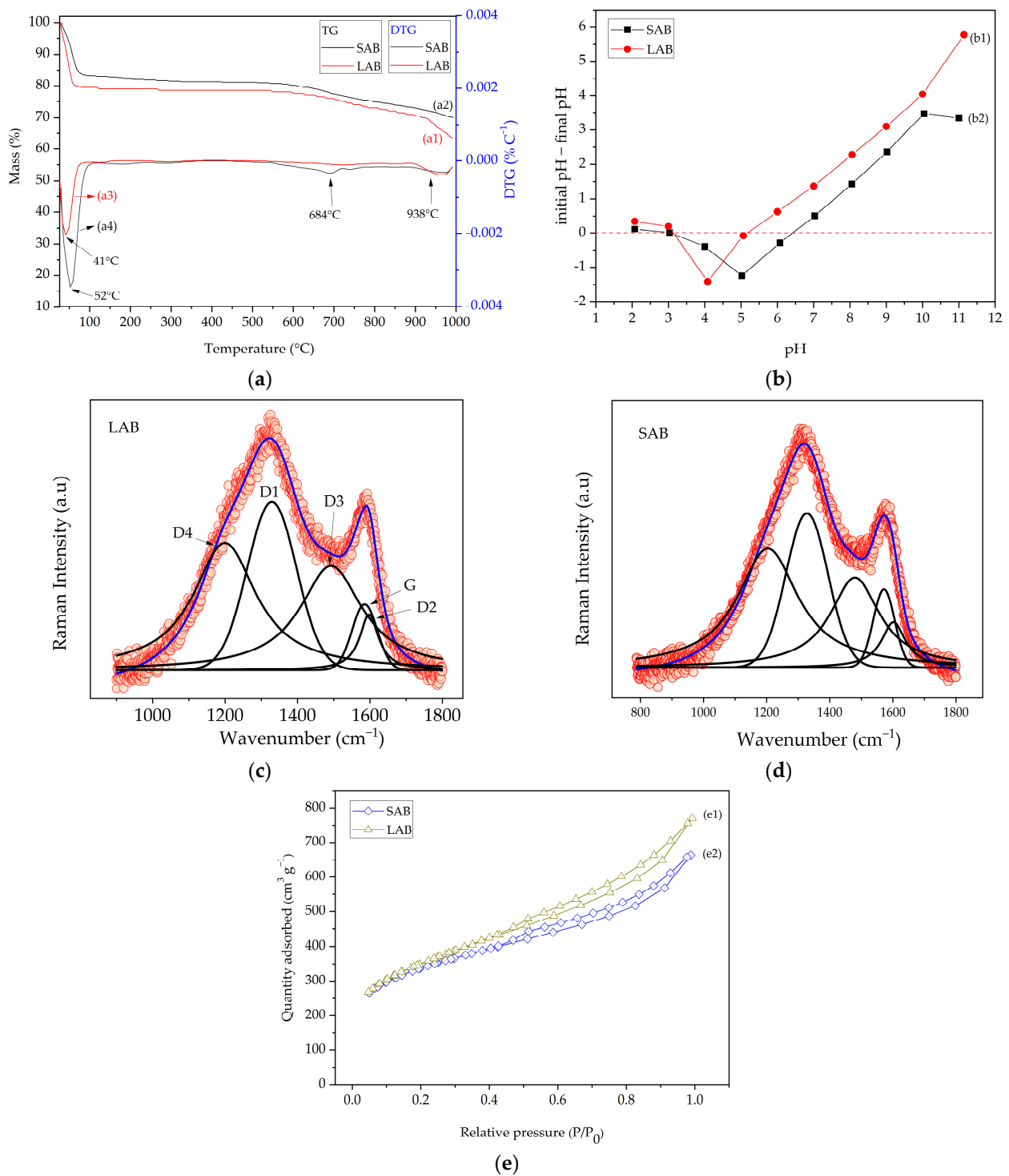
Figure 3. (**a**) Thermogravimetric curves: (**a1**) LAB and (**a2**) SAB; DTG: (**a3**) LAB and (**a4**) SAB; (**b**) pH_{pzc}: (**b1**) LAB and (**b2**) SAB; Raman spectrum of biochar: (**c**) LAB and (**d**) SAB; (**e**) nitrogen adsorption-desorption curves: (**e1**) LAB and (**e2**) SAB.

The ratio between the intensities of the D_1 and G peaks (I_{D1}/I_G) is applied to calculate the degree of imperfections (D_1 peaks) and the graphitic arrangements (G peaks) of the adsorbents before and after dye adsorption [77]. The ratio (I_{D1}/G_I) is shown in Table 1.

Table 1. Band intensity ratio (I_{D1}/I_G) for the SAB and LAB biochars.

Band	LAB			SAB		
	Amplitude	Center	FWHM	Amplitude	Center	FWHM
D_1	49.76	1329.19	160.25	185.79	1327.66	157.22
G	19.48	1585.40	81.73	94.31	1571.73	80.07
I_{D1}/I_G		2.55			1.96	

The ratio of the intensity of the D_1 band to G (I_{D1}/I_G) was observed to be 2.55 for the LAB and 1.96 for the SAB, indicating that the degree of imperfections (D_1 peaks) is superior to graphitic arrangements [78]. From these data, it is possible to suggest the presence of a more significant disorder of the carbon structure resulting from the activation process by $ZnCl_2$ [74].

The I_{D1}/I_G ratio shows that the carbon in biochars is partially graphitized and exists mainly in the form of amorphous carbon with a large pore structure [79], corroborating the XRD analysis. The I_{D1}/I_G value of the LAB (2.55) was higher than that of the SAB (1.96). It shows that the leaf biochar has more defective structures than the stem. In summary, the LAB presents a lower degree of graphitization, which generates more defect structures and increases porosity, which favors adsorption [80]. This result is confirmed in the BET analysis (Table 2), which indicated a slightly higher amount of pore volume in the LAB (1.072) compared to the SAB (0.939).

Table 2. Texture characteristics of the SAB and LAB adsorbents.

Samples	Surface Area ($m^2\ g^{-1}$)	Pore Volume ($cm^3\ g^{-1}$)	Average Pore Diameter (nm)
LAB	1195.00	1.072	1.614
SAB	1121.00	0.939	1.688

The nitrogen (N_2) adsorption/desorption isotherms for the LAB and SAB are shown in Figure 3e. The two isotherms can be classified as Type IV, which indicates monolayer-multilayer adsorption on both adsorbents [81] with a hysteresis loop at high relative pressure [82]. These reports indicate microporous structures [63] and mesoporous structures for both the SAB and LAB [83]. In the lower pressure range ($0 < P/P_0 < 0.2$), the volume adsorption of nitrogen increased smoothly, showing monolayer adsorption. The gas adsorption gradually increased in the range of $0.2 < P/P0 < 0.8$, indicating that the monolayer adsorption was shifted to a multilayer. Finally, in the range of $0.8 < P/P_0 < 1.0$, gas adsorption increased rapidly, suggesting that the phenomenon of capillary condensation occurs in adsorption [84]. The values of the texture characteristics of the LAB and SAB adsorbents are shown in Table 2.

The surface area calculated by the BET method, the pore volume, and the average diameter were close. Therefore, it is evident that the biochars are similar, and the adsorbent particles smaller than 2 nm indicate a microporous material [83], as was also confirmed in the morphology analysis [85].

Despite the similarity, discreet differences can be verified in each biochar. The XRD patterns of the LAB and SAB exhibit a broad peak between 20 and 30° for both. The SAB peaks at 25.3° while the LAB peaks at 25.0°, demonstrating that the degree of graphitization of the SAB is slightly more substantial than the LAB. It is inferred that, under the same synthesis conditions, the textural discrepancy of the water hyacinth stem and leaf should be responsible for the difference in the degree of graphitization because different plant parts have developed different microscopic structures due to different functions, which is a classic example of the perfect integration of function and structure. Therefore, biochar prepared from different biomasses must inherit the fine structure of its raw material and exhibit different adsorption and catalytic properties [86].

Furthermore, in the thermogravimetric analysis, the residual content of the SAB is relatively higher than the LAB's due to the higher amount of lignin in the first biochar [70]. Finally, by analyzing the distribution of the surface area and pore volume, it can be concluded that the two materials include micropores (pore size < 2 nm) and mesopores (2 nm < pore size < 50 nm). However, the LAB presents a slight increase in these structures compared to the SAB [86]. The surface area, the pore volume, and size distribution depend on the biochar preparation and the thermal conversion technique [87].

The analysis of fresh leaves of water hyacinth in a previous study determined that this part of the plant has a relatively large surface area with many evenly distributed in the epidermis [88]. The presence of this structure in the leaf is likely responsible for slightly increasing the surface area and pore volume after the carbonization process. A study aiming to build a biochar based on used tea leaves (FCU) for efficient adsorption and removal of low-level antibiotics in water analyzed the morphologies of FCU before and after heat treatment, characterized by SEM. The authors found that the FCU exhibited a rough surface with many obvious cracks and open stomata. With pyrolysis, they found that the stomata of the leaves opened more, and many pores formed entirely due to dehydration after heat treatment [89].

A review study carried out recently to analyze previous reports on the use of water hyacinth (in natural and carbonized form) as an adsorbent of heavy metal cations and textile dyes showed that the carbon derived from the water hyacinth leaf is a better adsorbent than the in the natural biomass of this plant [33]. Raw leaves have an irregular structure with rough pores, while leaf-derived biochar has more micropores with a well-defined structure. The available pores contribute to the adsorption of the dyes [90].

When the results consider the degree of graphitization, surface area, and pore volume, it is assumed that the excellent balance in the developed biochars is responsible for the equivalence of the adsorptive capacity between the LAB and SAB since both presented approximately the same amount of dye removed. The results obtained for the biochars can be compared with those of other adsorbents found in the literature (Table 3).

Table 3. Characteristics of the activated biochars used in the adsorption of dyes.

Samples	Surface Area ($m^2\ g^{-1}$)	Pore Volume ($cm^3\ g^{-1}$)	Average Pore Diameter (nm)	References
Pterospermum acerifolium	64.79	1.190	3.235	[84]
African Almond (*Terminalia catappa* L.)	816.00	0.360	2.000	[90]
Rice	27.32	-	9.369	[91]
Phragmites karka	659.20	0.169	0.500	[92]
Pine	159.42	0.114	2.880	[93]
Eichhornia crassipes	124.67	0.065	4.150	[63]
Eichhornia crassipes	192.50	0.380	-	[23]
Livistona chinensis	43.25	0.054	5.057	[28]
LAB	1195.00	1.072	1.614	This study
SAB	1121.00	0.939	1.688	This study

The surface area and pore volumes differed slightly between the biochars analyzed. However, the LAB and SAB characteristics were relatively superior in most studies. Notably, pore formation is mainly due to the loss of volatile matter from the biochar surface during pyrolysis, and untreated biochar (without activation) has fewer pores. On the contrary, porosity increases in the case of biochar treated with reagents [87]. Such issues need to be considered in this correlation.

3.2. Adsorption Experiments

The initial pH of a solution is a parameter that influences the ionization balance of the species, as well as the surface charges of the adsorbent, generating changes in the adsorption capacity [24]. Therefore, the initial pH's effects on the MB dye adsorption on the LAB and SAB surface were investigated on a scale of pH values 4, 7, and 10 (Figure 4).
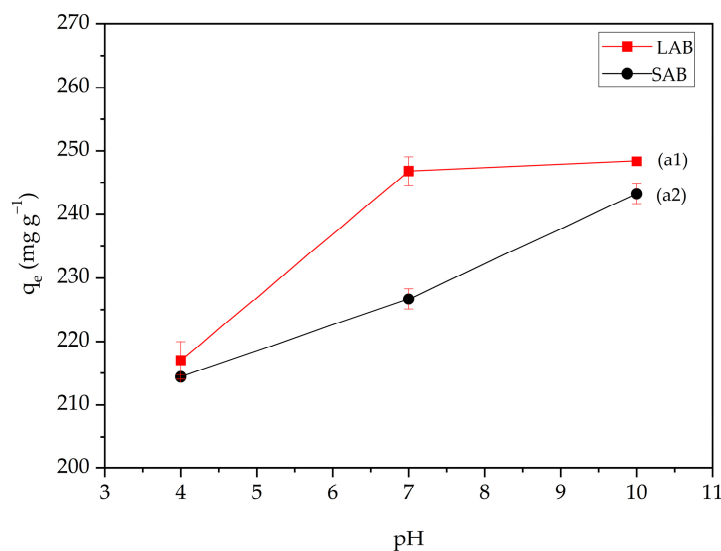

Figure 4. Effect of pH on MB adsorption capacity in LAB (**a1**) and SAB (**a2**).

Figure 4 indicates that the adsorption of the MB dye is lower for acidic pH (pH 4), 217.00 mg g^{-1} for the LAB, and 214.00 mg g^{-1} for the SAB. This low adsorption of MB can be explained by low pH values, which indicate the gradual formation of a positive charge on the surface, which weakens interactions and increases the affinity with the solvent, preventing the dye's adsorption [31]. Furthermore, the effectiveness of the dye may be lower at low pH values due to competition between H$^+$ ions and the protonated ions of the dye at adsorption sites [94].

At the same time, it is noted that the amount of MB removal for the LAB increases as the pH of the solution increases, from pH 4 to pH 7, with no significant changes being observed in the adsorption capacity of the MB above pH 7 [95]. The maximum amount of removal for the LAB was at pH 7 with 246.00 mg g^{-1}. In the higher pH range (pH > 7), the amount of removal remained practically the same due to the abundant availability of hydroxyl ions and encounter with the dye molecules for the active sites of the activated biochars [96].

For the SAB, the MB removal is maximum at pH 10, reaching 243.00 mg g^{-1}, which means that the MB adsorption rate increased with increasing pH [97]. This increase in adsorption capacity between the adsorbent and the dye is due to the groups present on the surface of activated biochars, which are negatively charged, in addition to the pH$_{pzc}$ values, which favor the removal of the MB, mainly through electrostatic interactions between activated biochars and adsorbate ions that make it significant [98]. It indicates that pH > pH$_{pzc}$ is favorable for the adsorption of MB and other dyes with similar charges and structures from textile industrial effluents [99].

It can be observed that the adsorption mechanism in adsorbent materials (LAB and SAB) is mainly based on electrostatic interactions, which are influenced by the pH of the solution. Electrostatic interactions occur due to electrical charges on the adsorbent surface and the MB dye ions, as presented above. Furthermore, hydrogen, hydrophobic, and π-π interactions may also occur between the adsorbents (LAB and SAB) and the MB dye, as shown in Figure 5.
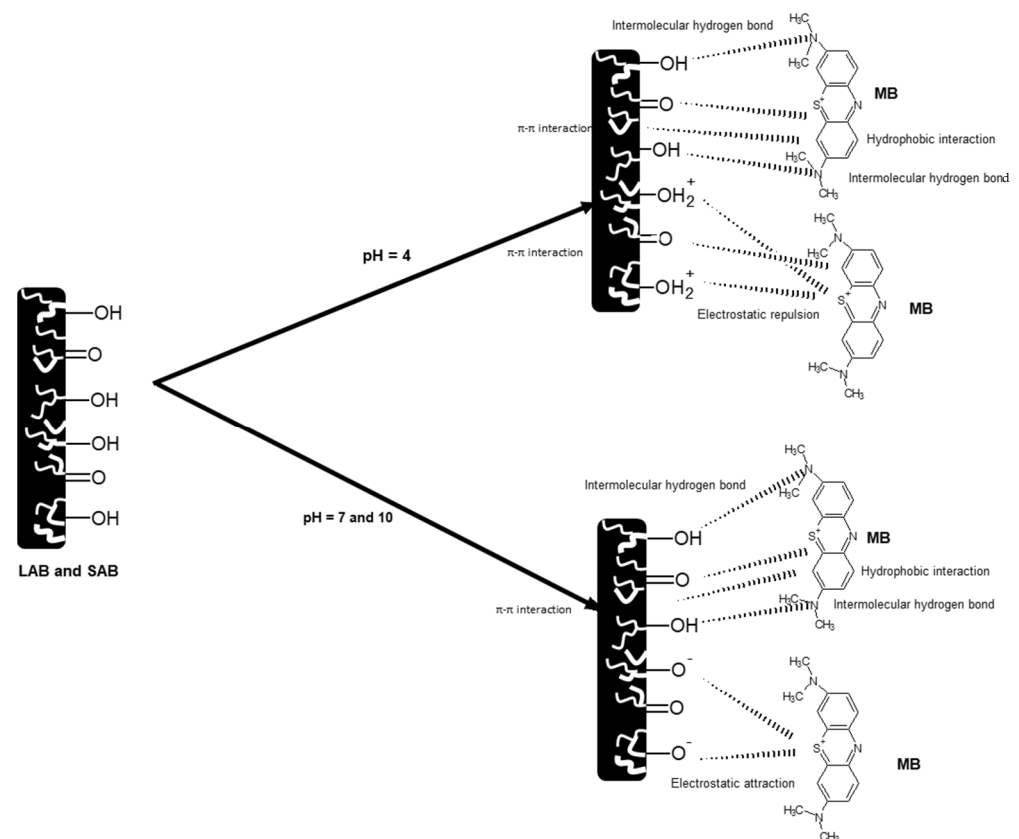
Figure 5. Adsorption mechanism of the adsorbent materials (LAB and SAB) based on the study of pH and pH_{pzc}.

Hakami [100] found that with increasing pH value, the adsorbent surfaces became negatively charged, resulting in a greater adsorption capacity of the sample due to the formation of an electrostatic interaction between the negatively charged activated biochar surfaces and the positively charged MB dye (Figure 6).
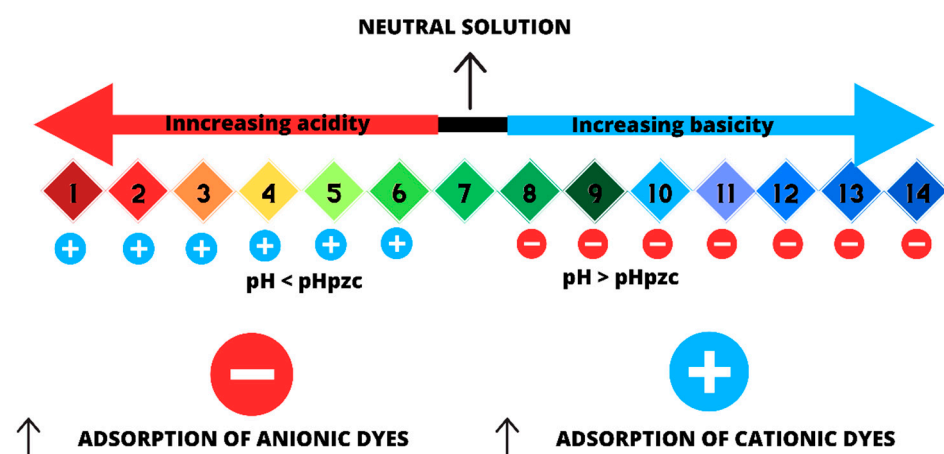
**Figure 6.** Relationship between pH and pH_{pzc}. Source: own authorship.

The efficiency of MB adsorption by the LAB and SAB, as a function of contact time with an initial concentration of 700.00 mg L^{-1} at a temperature of 25 °C, is shown in Figure 7. It is possible to observe the fastest adsorption in the first 55 min. The LAB and SAB removed approximately 255 mg g^{-1} and 248 mg g^{-1} of MB, respectively, indicating that the adsorption is very close for both. Then, the velocity gradually decreases until

equilibrium is reached, where there is no change in concentration for the LAB and SAB. These results signal a fast and highly favorable interaction.
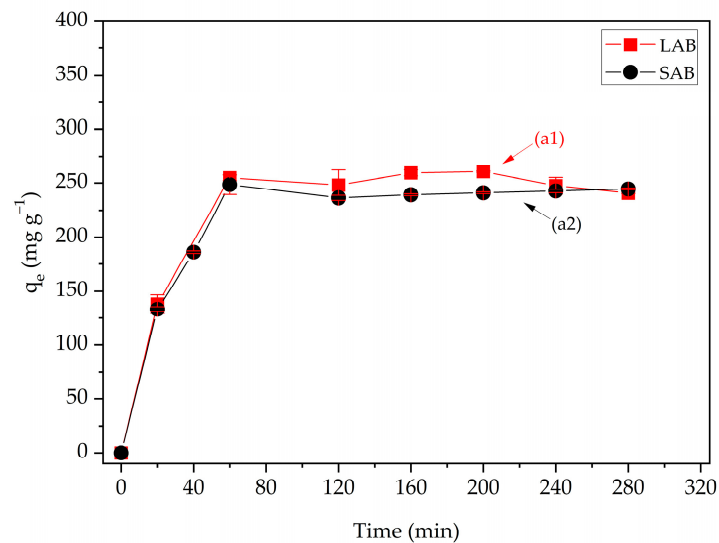
Figure 7. Time isotherm for the removal of MB by the LAB (**a1**) and SAB (**a2**).

From the data presented in Figure 7, it was possible to evaluate the fit of the points to the pseudo-first-order and pseudo-second-order models to verify the most appropriate mechanism to describe the adsorption of MB by the LAB and SAB. The results are shown in Figure 8, and the kinetic parameters are in Table 4.
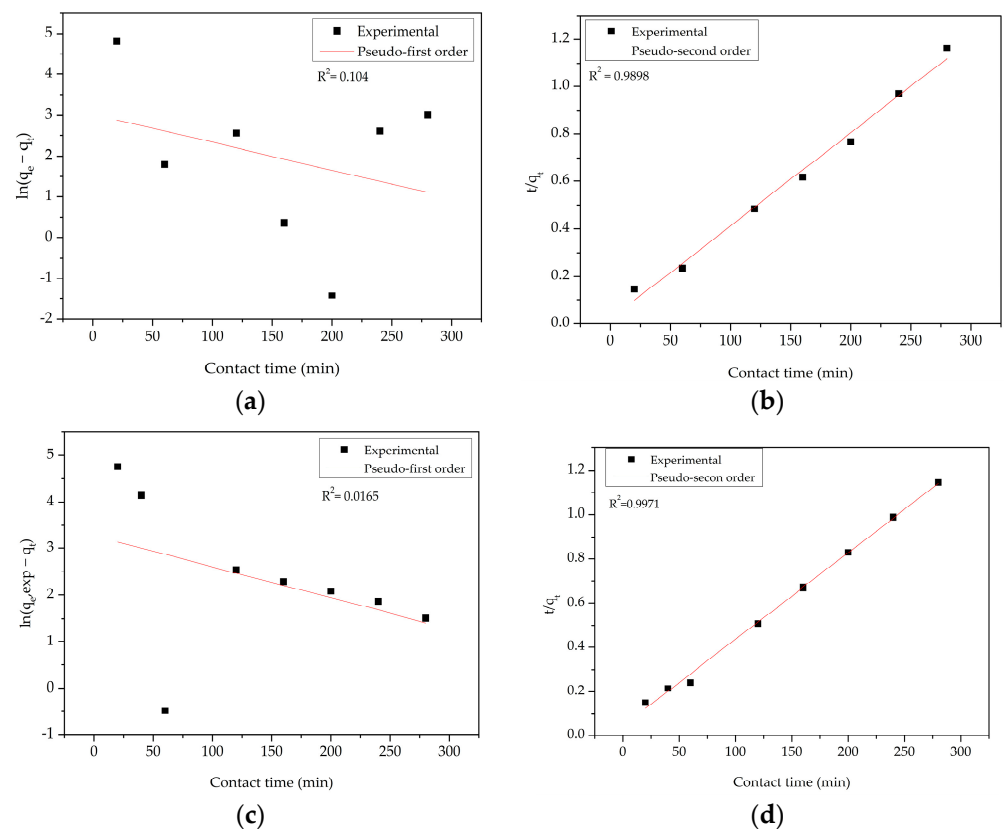
Figure 8. Adsorption kinetics for the LAB: (**a**) pseudo-first-order and (**b**) pseudo-second-order at 25 °C. For the SAB: (**c**) pseudo-first-order and (**d**) pseudo-second-order at 25 °C.

Table 4. Kinetic parameters of the LAB and SAB.

Ads	Pseudo-First-Order			Pseudo-Second-Order		
	q_e (mg g^{-1})	K_1 (min^{-1})	R^2	q_e (mg g^{-1})	K_2 (mg g^{-1} min^{-1})	R^2
LAB	20.44	0.0068	0.104	254.453	0.000788	0.9898
SAB	26.13	0.0066	0.0165	253.807	0.000338	0.9971

q_e amount of dye adsorbed in equilibrium (mg g^{-1}); adsorption constant K_1 of the first-order model (min^{-1}); second-order model constant K_2 (mg g^{-1} min^{-1}) and linearity coefficient R^2.

In the study of adsorption kinetics, the data shown in Figure 8 better fit the pseudo-second-order model for the LAB and SAB, obtaining correlation coefficients of 0.9898 and 0.9971, respectively [25]. Thus, it is determined that the adsorption phenomenon may be chemisorption [101]. Furthermore, it implies that the pseudo-second-order kinetic model best describes the adsorption kinetics of the MB dye by the developed biochars [45].

Another analysis can be interpreted by comparing the fit parameters in Table 4. From these fits obtained and the correlation coefficient, it was established that the pseudo-second-order model describes the behavior of the adsorption process [63]. Therefore, it was established that both biochars could adsorb MB and that chemisorption occurs due to the formation of chemical interactions between the adsorbent and adsorbate on the surface [102].

Isothermal analyses are relevant in studying the adsorption data instrument [103]. Many adsorption isotherms have been used to fit experimental equilibrium adsorption data [104]. In the present study, the Langmuir and Freundlich models were used because they can predict the experimental data's behavior. The experimental isotherms of the MB were obtained by plotting the results found, as shown in Figure 9.
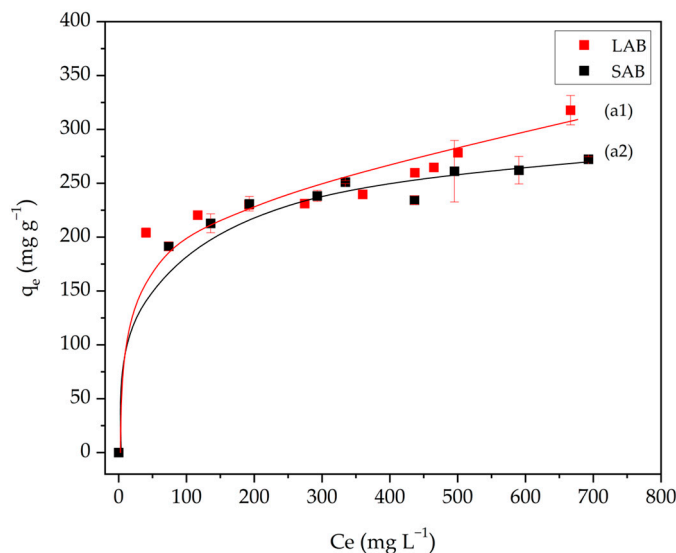
Figure 9. MB adsorption isotherm for the LAB (**a1**) and SAB (**a2**).

The plotted values indicate that the adsorption for the LAB and SAB is favorable, outlining that the adsorptive process will occur even at low concentrations.

It was possible to adjust the experimental data to the Freundlich and Langmuir models for the LAB (Figure 10a,b) and SAB (Figure 10c,d), both in linearized form. The isotherm parameters are shown in Table 5, and the linear models were compared using the R^2 value as a reference.
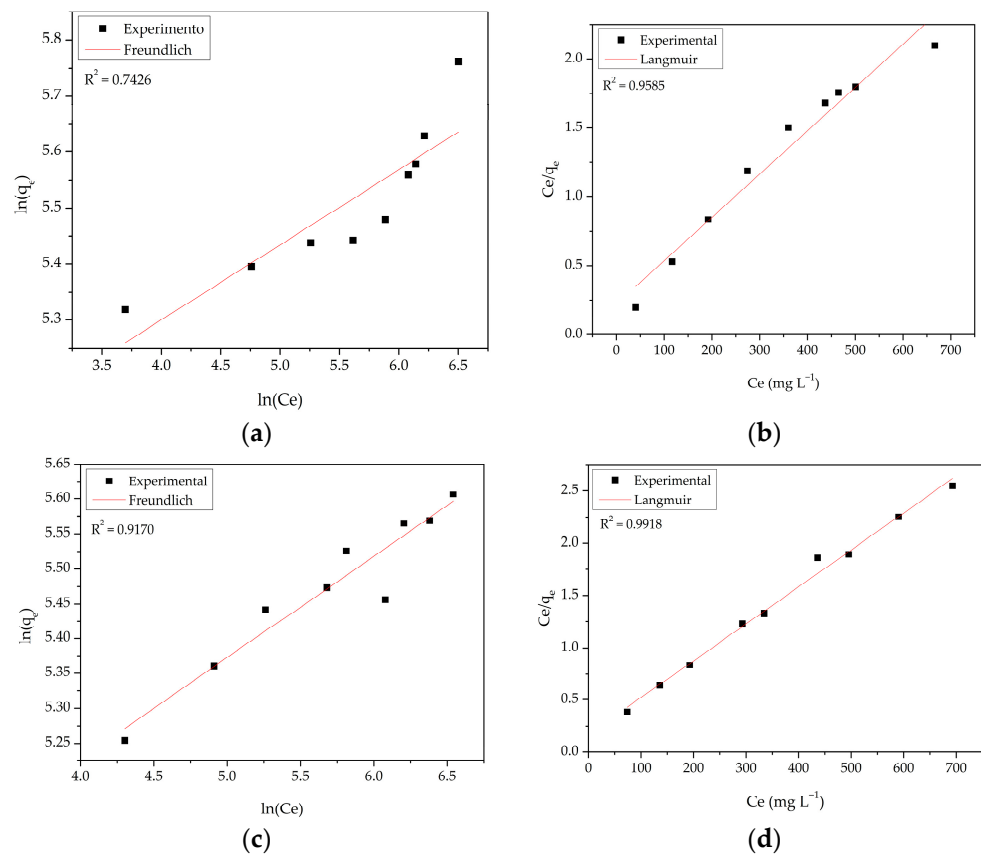
Figure 10. Linearized isotherm of (**a**) Freundlich and (**b**) Langmuir for the LAB adsorption; linearized isotherm of (**c**) Freundlich and (**d**) Langmuir for the SAB adsorption.

Table 5. Constant of the LAB and SAB isothermal models.

	Freundlich			Langmuir		
Ads	n	K_F (mg L^{-1})	R^2	q_{max} (mg g^{-1})	K_L (mg g^{-1})	R^2
LAB	7.45	117.19	0.7426	322.58	0.0139	0.9585
SAB	6.88	104.17	0.9170	285.71	0.0208	0.9918

q_{max} maximum amount of adsorbed species per mass of bioadsorbent (mg g^{-1}); constant $1/n$ related to surface heterogeneity; K_L Langmuir adsorption constant in the chemical equilibrium between the adsorbate and the adsorbent (mg L^{-1}); adsorption constant related to adsorption capacity and linearity coefficient R^2.

Figure 10 determines a better fit of the adsorption data to the Langmuir model with higher linearity values than the Freundlich model for the LAB and SAB [105]. This model assumes MB adsorption by activated biochars occurs in monolayers and homogeneous sites with the same binding energy [106]. This hypothesis is supported by the FTIR results found in Figure 1b, in which the signals indicate the presence of hydroxyl and carbonyl groups, reducing the number of active sites on the surface [69]. The Langmuir model was observed in other adsorption studies using activated biochars, highlighted below.

Durrani et al. [107] performed isothermal tests using date palm-activated biochar for the adsorption of MB in water, whose values described the best result for Langmuir, where the maximum MB adsorption capacity was 666.00 mg g^{-1}. Similarly, the study by Trung Hiep et al. [108] presented isotherm tests using biochar from the *Sesbania sesban* plant for the removal of MB in water. The results were best fitted to the Langmuir model, and its maximum adsorption capacity was 6.60 mg g^{-1}. As well as the system of Sulaiman et al. [109], who verified the isotherms of activated cassava stem biochar, in which the

equilibrium data were better adjusted to the Langmuir, with a maximum amount of 384.61 mg g^{-1}.

3.3. Characterization of Activated Biochars after Adsorption

Characterizations of activated biochars after adsorption were performed to understand better how this process would affect the studied materials; the same acronyms were used, with A at the end of the acronyms of the material. Thus, the materials after adsorption are called biochar activated from leaf-activated biochar after adsorption (LABA) and stem after adsorption (SABA).

After adsorption, in the XRD results in Figure 11(a1,a2), it is observed that there were no changes in the structure of the materials compared to Figure 1(a1,a2) and that the typical peak of the adsorption characteristic of the structure of the graphite remains in the same region 2 θ = 20–30° [97].

Figure 11(b1,b2) shows FTIR spectra to characterize the surface functional groups after adsorption. It is observed that after MB adsorption, the number of bands around 2980 cm^{-1} disappeared, while some new bands were identified in the range of 1130 and 890 cm^{-1}, both for the SABA and LABA [73]. After MB adsorption, the band at 3400 cm^{-1} is attributed to the stretching vibration (OH) [97]. The band of around 1600 cm^{-1} reflects the stretching (C=C) of aromatic groups [110]. In bands between the 1400–1300 cm^{-1} (C=O) and 1130–890 cm^{-1} groups, asymmetric stretching vibrations of the C–O–C bond are found on the surface of the material [111], which are responsible for the adsorption of the MB dye [112].

The Raman spectra of the SABA and LABA found in Figure 11c,d, respectively, after adsorption, consisted mainly of D$_1$ = 1350 cm^{-1} (non-graphitic carbon) and G = 1580 cm^{-1} (graphitic carbon) [57]. The band intensity ratio (I$_{D1}$/I$_G$) for the SABA and LABA biochars is found in Table 6.

**Table 6.** Intensity ratio of the I$_{D1}$/I$_G$ bands for the SABA and LABA biochars.

Band	SABA			LABA		
	Amplitude	Center	FWHM	Amplitude	Center	FWHM
D$_1$	225.18	1344.61	178.98	183.54	1320.66	179.65
G	107.74	1577.12	61.15	68.77	1575.32	93.31
I$_{D1}$/I$_G$		2.09			2.66	

The results of the intensity ratio of the D$_1$ to G band (I$_{D1}$/I$_G$) of the LAB and SAB before adsorption were 2.55 and 1.96, respectively (Table 1). It confirms a disorder in the structure of biochars [113], which is suitable for the adsorption process of the AM dye [77]. After the adsorption of dye molecules, the ID1/IG intensity ratio increased further to 2.66 (LABA) and 2.09 (SABA) (Table 6), suggesting the interaction between the MB dye and biochar [76].

After the adsorption process, a BET analysis was performed to examine the change in surface area and the adsorption/desorption curve. Figure 11(e1,e2) represents the adsorption/desorption curve of the biochars with the MB dye. It is noticed that both adsorbents after MB adsorption follow a type IV isotherm with a hysteresis loop at high relative pressure. The texture characteristic values of the LABA and SABA adsorbents after adsorption are shown in Table 7.

Table 7. Texture characteristics of the LABA and SABA adsorbents.

Samples	Surface Area (m^2 g^{-1})	Pore Volume (cm^3 g^{-1})	Average Pore Diameter (nm)
LABA	713.00	0.926	2.769
SABA	615.90	0.728	2.769
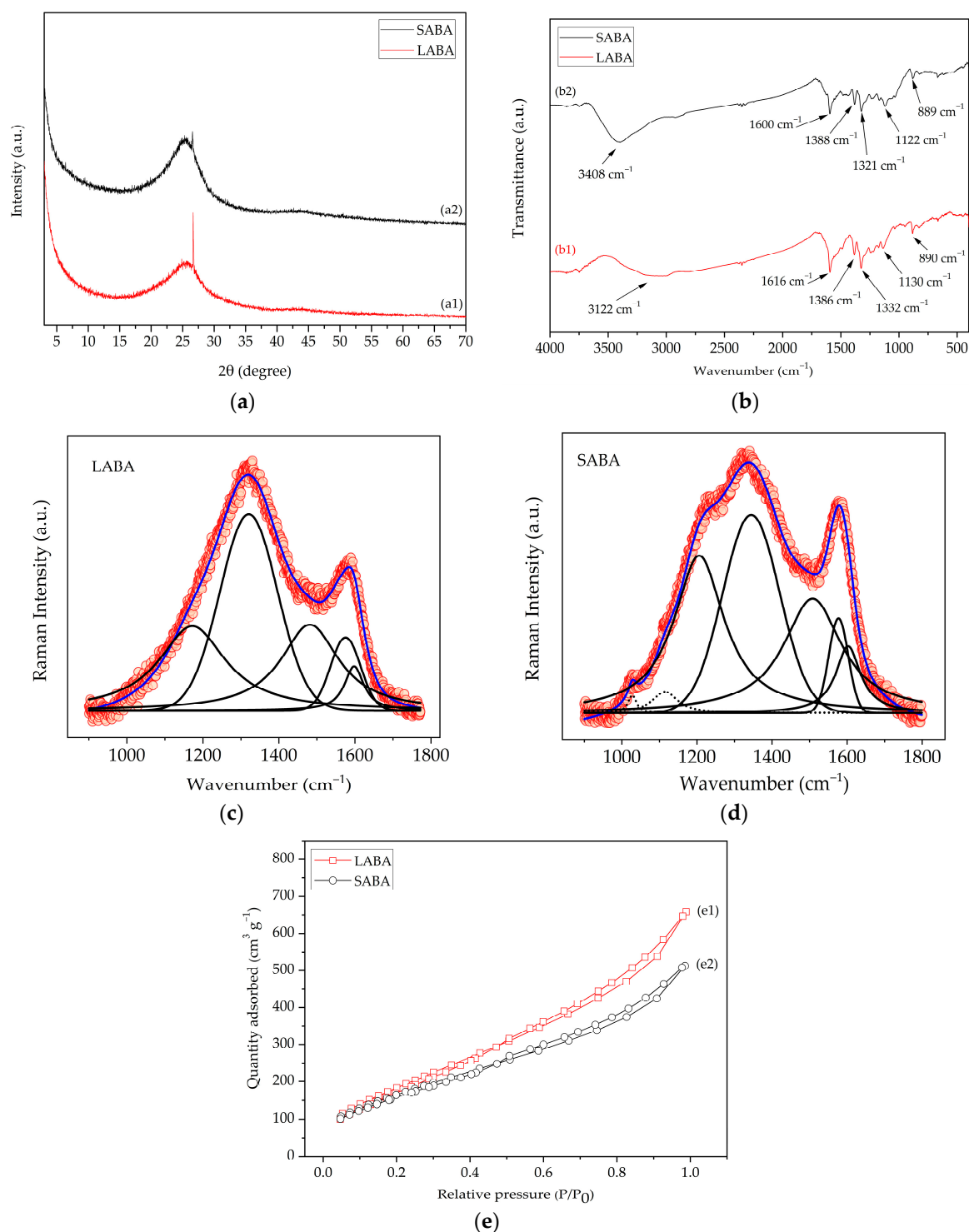
Figure 11. (**a**) X-ray diffraction patterns of activated biochar from the leaf of the water hy-acinth after adsorption of the dye MB (LABA) and activated biochar from the stem of the water hy-acinth after adsorption of the dye MB (SABA): (**a1**) LABA and (**a2**) SABA. FTIR spectrum of biochars activated after MB adsorption: (**b1**) LABA and (**b2**) SABA; Result of Raman characterization for activated biochars after adsorption: (**c**) LABA and (**d**) SABA; (**e**) BET surface area analysis, Adsorption-desorption isotherms of biochars activated after adsorption: (**e1**) LABA and (**e2**) SABA.

The results in Table 7, compared with Table 2, show that pore volumes decreased from 0.939 to 0.728 cm^3 g^{-1} (SABA) and from 1.072 to 0.926 cm^3 g^{-1} (LABA), suggesting that the

MB dye partially filled the pores. Therefore, the surface area of the biochars was reduced from 1121.00 to 615.90 m^2 g^{-1} (SABA) and from 1195.00 to 713.00 m^2 g^{-1} (LABA) [84].

3.4. Comparison of the Adsorption Capacity of LAB e SAB with Other Adsorbents

Several studies have studied MB dye adsorption using different types of adsorbents. Table 8 compares the maximum adsorption capacities of this dye by the LAB and SAB with other adsorbents from previous studies. The LAB and SAB have adequate adsorption capacity for MB.

Table 8. Comparison of MB adsorption capacity by the LAB and SAB to other adsorbents found in the recent literature.

Adsorbent	q_{max} (mg g^{-1})	References
Biochar activated—*P. juliflora* pods	54.73	[114]
Biochar activated—*Coriandrum sativum*	94.90	[59]
Biochar activated mesoporous via microwave process	186.40	[112]
Biochar activated—*Pterospermum acerifolium*	166.65	[84]
Biochar activated—Eucalyptus	49.61	[115]
Biochar activated—Cassava (*Manihot esculenta* Crantz)	194.58	[116]
Biochar activated—Arjun Bark Powder	68.30	[117]
Biochar activated—pine needles	277.78	[118]
Biochar activated—*Juglans regia*	102.28	[119]
Biochar activated—sugar cane bagasse	163.93	[120]
LAB	322.58	This study
SAB	285.71	This study

4. Conclusions

The LAB and SAB biochars showed a predominantly amorphous structure, indicating the existence of graphitic carbon that can be formed during the decomposition of the material. In the analysis of the FTIR spectra of the parts of the biochars, it was possible to observe a few peaks, warning of the existence of a small variety of surface groups. The morphological structures of the LAB and SAB showed numerous irregular and porous cavities.

The TG data confirms that the mass loss was slight in the temperature range 100–800 °C. Below this temperature, the event refers to the physisorption of water molecules and the environment. The process above the temperature used for activation occurs, confirming the activation process. Raman confirmed the disorder in the structure of the biochars. The surface area, the pore volume, and average pore diameter were 1195.00 m^2 g^{-1}, 1.072 cm^3 g^{-1}, and 1.614 nm for the LAB and 1121.00 m^2 g^{-1}, 0.939 cm^3 g^{-1}, and 1.688 nm for the SAB.

The adsorbents LAB and SAB demonstrated efficiency in removing methylene blue over time (with adsorption of 255 mg g^{-1} and 248 mg g^{-1} of MB, for the LAB and SAB, respectively) following the pseudo-second-order model. Equilibrium studies revealed that both adsorbents favor adsorption, with a better correspondence to the Langmuir model (R^2 = 0.9585 and 0.9918 for LAB and SAB, respectively) compared to the Freundlich model. These results suggest that activated biochar produced from water hyacinth can be successfully used in wastewater treatment, offering a viable solution for pollutant removal.

Author Contributions: Conceptualization: M.T.C., A.Í.S.M., A.L.F.d.C.M. and E.C.S.-F.; methodology: M.T.C., A.Í.S.M., A.L.F.d.C.M. and F.J.L.F.; software: M.T.C., A.Í.S.M. and A.L.F.d.C.M.; validation: M.T.C., A.Í.S.M., A.L.F.d.C.M. and R.D.S.B.; formal analysis, F.E.P.S. and R.D.S.B.; investigation: M.T.C., A.Í.S.M., F.J.L.F. and R.D.S.B.; resources: B.C.V., J.A.O., R.D.S.B., M.D.M.O.C., R.R.P.-G.,

References

1. El-Bery, H.M.; Saleh, M.; El-Gendy, R.A.; Saleh, M.R.; Thabet, S.M. High Adsorption Capacity of Phenol and Methylene Blue Using Activated Carbon Derived from Lignocellulosic Agriculture Wastes. *Sci. Rep.* **2022**, *12*, 5499. [CrossRef]
2. Yue, C.; Chen, L.; Zhang, H.; Huang, J.; Jiang, H.; Li, H.; Yang, S. Metal–Organic Framework-Based Materials: Emerging High-Efficiency Catalysts for the Heterogeneous Photocatalytic Degradation of Pollutants in Water. *Environ. Sci.* **2023**, *9*, 669–695. [CrossRef]
3. Nayak, S.S.; Mirgane, N.A.; Shivankar, V.S.; Pathade, K.B.; Wadhawa, G.C. Adsorption of Methylene Blue Dye over Activated Charcoal from the Fruit Peel of Plant Hydnocarpus Pentandra. *Mater. Today Proc.* **2021**, *37*, 2302–2305. [CrossRef]
4. Saeed, A.A.H.; Harun, N.Y.; Sufian, S.; Siyal, A.A.; Zulfiqar, M.; Bilad, M.R.; Vagananthan, A.; Al-Fakih, A.; Ghaleb, A.A.S.; Almahbashi, N. Eucheuma Cottonii Seaweed-Based Biochar for Adsorption of Methylene Blue Dye. *Sustainability* **2020**, *12*, 10318. [CrossRef]
5. Kucukcobanoglu, Y.; Ayisigi, M.; Haseki, S.; Aktas, L.Y. In Situ Green Synthesis of Cellulose Based Silver Nanocomposite and Its Catalytic Dye Removal Potential Against Methylene Blue. *J. Clust. Sci.* **2022**, *33*, 1623–1633. [CrossRef]
6. Akodad, M.; Baghour, M.; Moumen, A.; Skalli, A.; Azizi, G.; Anjjar, A.; Aalaoul, M.; Daoudi, I. Daoudi Adsorption of a Basic Dye, Methylene Blue, in Aqueous Solution on Bentonite. *Moroc. J. Chem.* **2021**, *9*, 416–433.
7. Wang, J.; Dai, L.; Liu, Y.; Li, R.; Yang, X.; Lan, G.; Qiu, H.; Xu, B. Adsorption Properties of β-Cyclodextrin Modified Hydrogel for Methylene Blue. *Carbohydr. Res.* **2021**, *501*, 108276. [CrossRef]
8. Bhavani, P.; Hussain, M.; Park, Y.-K. Recent Advancements on the Sustainable Biochar Based Semiconducting Materials for Photocatalytic Applications: A State of the Art Review. *J. Clean. Prod.* **2022**, *330*, 129899. [CrossRef]
9. Khalil, A.M.; Kenawy, S.H. Hybrid Membranes Based on Clay-Polymer for Removing Methylene Blue from Water. *Acta Chim. Slov.* **2020**, *67*, 96–104. [CrossRef]
10. Iwuozor, K.O.; Ighalo, J.O.; Ogunfowora, L.A.; Adeniyi, A.G.; Igwegbe, C.A. An Empirical Literature Analysis of Adsorbent Performance for Methylene Blue Uptake from Aqueous Media. *J. Environ. Chem. Eng.* **2021**, *9*, 105658. [CrossRef]
11. Kasinathan, M.; Thiripuranthagan, S.; Sivakumar, A. Fabrication of Sphere-like Bi2MoO6/ZnO Composite Catalyst with Strong Photocatalytic Behavior for the Detoxification of Harmful Organic Dyes. *Opt. Mater.* **2020**, *109*, 110218. [CrossRef]
12. Xiong, Z.-M.; O'Donovan, M.; Sun, L.; Choi, J.Y.; Ren, M.; Cao, K. Anti-Aging Potentials of Methylene Blue for Human Skin Longevity. *Sci. Rep.* **2017**, *7*, 2475. [CrossRef]
13. Al-Wasidi, A.S.; AlZahrani, I.I.S.; Thawibaraka, H.I.; Naglah, A.M.; El-Desouky, M.G.; El-Bindary, M.A. Adsorption Studies of Carbon Dioxide and Anionic Dye on Green Adsorbent. *J. Mol. Struct.* **2022**, *1250*, 131736. [CrossRef]
14. Chen, L.; Li, F.; Wei, Y.; Li, G.; Shen, K.; He, H.-J. High Cadmium Adsorption on Nanoscale Zero-Valent Iron Coated *Eichhornia crassipes* Biochar. *Environ. Chem. Lett.* **2019**, *17*, 589–594. [CrossRef]
15. Rashed, M.N.; El Taher, M.A.; Fadlalla, S.M. Fadlalla Synthesis and Photocatlytic Application of Drinking Water Treatment Sludge@ TiO_2 Composite for Degradation of Methylene Blue Dye. *Pollution* **2020**, *6*, 785–799.
16. Jawad, A.H.; Saud Abdulhameed, A.; Wilson, L.D.; Syed-Hassan, S.S.A.; ALOthman, Z.A.; Rizwan Khan, M. High Surface Area and Mesoporous Activated Carbon from KOH-Activated Dragon Fruit Peels for Methylene Blue Dye Adsorption: Optimization and Mechanism Study. *Chin. J. Chem. Eng.* **2021**, *32*, 281–290. [CrossRef]
17. Din, M.I.; Khalid, R.; Najeeb, J.; Hussain, Z. Fundamentals and Photocatalysis of Methylene Blue Dye Using Various Nanocatalytic Assemblies- a Critical Review. *J. Clean. Prod.* **2021**, *298*, 126567. [CrossRef]
18. Khan, I.; Saeed, K.; Zekker, I.; Zhang, B.; Hendi, A.H.; Ahmad, A.; Ahmad, S.; Zada, N.; Ahmad, H.; Shah, L.A.; et al. Review on Methylene Blue: Its Properties, Uses, Toxicity and Photodegradation. *Water* **2022**, *14*, 242. [CrossRef]

19. Wang, H.; Xu, J.; Liu, X.; Sheng, L. Preparation of Straw Activated Carbon and Its Application in Wastewater Treatment: A Review. *J. Clean. Prod.* **2021**, *283*, 124671. [CrossRef]

20. Silva, M.C.; Spessato, L.; Silva, T.L.; Lopes, G.K.P.; Zanella, H.G.; Yokoyama, J.T.C.; Cazetta, A.L.; Almeida, V.C. H_3PO_4–Activated Carbon Fibers of High Surface Area from Banana Tree Pseudo-Stem Fibers: Adsorption Studies of Methylene Blue Dye in Batch and Fixed Bed Systems. *J. Mol. Liq.* **2021**, *324*, 114771. [CrossRef]

21. Jawad, A.H.; Abdulhameed, A.S.; Bahrudin, N.N.; Hum, N.N.M.F.; Surip, S.N.; Syed-Hassan, S.S.A.; Yousif, E.; Sabar, S. Microporous Activated Carbon Developed from KOH Activated Biomass Waste: Surface Mechanistic Study of Methylene Blue Dye Adsorption. *Water Sci. Technol.* **2021**, *84*, 1858–1872. [CrossRef]

22. Lütke, S.F.; Igansi, A.V.; Pegoraro, L.; Dotto, G.L.; Pinto, L.A.A.; Cadaval, T.R.S. Preparation of Activated Carbon from Black Wattle Bark Waste and Its Application for Phenol Adsorption. *J. Environ. Chem. Eng.* **2019**, *7*, 103396. [CrossRef]

23. Kabir, M.M.; Alam, F.; Akter, M.M.; Gilroyed, B.H.; Didar-ul-Alam, M.; Tijing, L.; Shon, H.K. Highly Effective Water Hyacinth (*Eichhornia crassipes*) Waste-Based Functionalized Sustainable Green Adsorbents for Antibiotic Remediation from Wastewater. *Chemosphere* **2022**, *304*, 135293. [CrossRef] [PubMed]

24. Ramirez-Muñoz, A.; Pérez, S.; Flórez, E.; Acelas, N. Recovering Phosphorus from Aqueous Solutions Using Water Hyacinth (*Eichhornia crassipes*) toward Sustainability through Its Transformation to Apatite. *J. Environ. Chem. Eng.* **2021**, *9*, 106225. [CrossRef]

25. Prasad, R.; Sharma, D.; Yadav, K.D.; Ibrahim, H. *Eichhornia crassipes* as Biosorbent for Industrial Wastewater Treatment: Equilibrium and Kinetic Studies. *Can. J. Chem. Eng.* **2022**, *100*, 439–450. [CrossRef]

26. Madikizela, L.M. Removal of Organic Pollutants in Water Using Water Hyacinth (*Eichhornia crassipes*). *J. Environ. Manag.* **2021**, *295*, 113153. [CrossRef] [PubMed]

27. González-García, P.; Gamboa-González, S.; Andrade Martínez, I.; Hernández-Quiroz, T. Preparation of Activated Carbon from Water Hyacinth Stems by Chemical Activation with K_2CO_3 and Its Performance as Adsorbent of Sodium Naproxen. *Environ. Prog. Sustain. Energy* **2020**, *39*, e13366. [CrossRef]

28. Giri, B.S.; Sonwani, R.K.; Varjani, S.; Chaurasia, D.; Varadavenkatesan, T.; Chaturvedi, P.; Yadav, S.; Katiyar, V.; Singh, R.S.; Pandey, A. Highly Efficient Bio-Adsorption of Malachite Green Using Chinese Fan-Palm Biochar (*Livistona chinensis*). *Chemosphere* **2022**, *287*, 132282. [CrossRef]

29. Zhuang, H.; Zhu, H.; Zhang, J.; Shan, S.; Fang, C.; Tang, H.; Xie, Q. Enhanced 2,4,6-Trichlorophenol Anaerobic Degradation by Fe3O4 Supported on Water Hyacinth Biochar for Triggering Direct Interspecies Electron Transfer and Its Use in Coal Gasification Wastewater Treatment. *Bioresour. Technol.* **2020**, *296*, 122306. [CrossRef]

30. Xu, Z.; Xing, Y.; Ren, A.; Ma, D.; Li, Y.; Hu, S. Study on Adsorption Properties of Water Hyacinth-Derived Biochar for Uranium (VI). *J. Radioanal. Nucl. Chem.* **2020**, *324*, 1317–1327. [CrossRef]

31. Bapat, S.A.; Jaspal, D.K. Surface-Modified Water Hyacinth (*Eichhornia crassipes*) over Activated Carbon for Wastewater Treatment: A Comparative Account. *S. Afr. J. Chem.* **2020**, *73*, 70–80. [CrossRef]

32. Li, F.; He, X.; Srishti, A.; Song, S.; Tan, H.T.W.; Sweeney, D.J.; Ghosh, S.; Wang, C.-H. Water Hyacinth for Energy and Environmental Applications: A Review. *Bioresour. Technol.* **2021**, *327*, 124809. [CrossRef] [PubMed]

33. Lima, H.d.P.; Asencios, Y.J.O. *Eichhornia crassipes* (Mart.) Solms (Natural or Carbonized) as Biosorbent to Remove Pollutants in Water. *SN Appl. Sci.* **2021**, *3*, 750. [CrossRef] [PubMed]

34. Yang, Y.; Cannon, F.S. Biomass Activated Carbon Derived from Pine Sawdust with Steam Bursting Pretreatment; Perfluorooctanoic Acid and Methylene Blue Adsorption. *Bioresour. Technol.* **2022**, *344*, 126161. [CrossRef]

35. Wang, Y.; Zhuang, Y.; Wang, S.; Liu, Y.; Kong, L.; Li, J.; Chen, H. Preparation and Characterization of Porous Palygorskite/Carbon Composites through Zinc Chloride Activation for Wastewater Treatment. *Clays Clay Miner.* **2022**, *70*, 450–459. [CrossRef]

36. Santhosh, A.; Dawn, S.S. Synthesis of Zinc Chloride Activated Eco-Friendly Nano-Adsorbent (Activated Carbon) from Food Waste for Removal of Pollutant from Biodiesel Wash Water. *Water Sci. Technol.* **2021**, *84*, 1170–1181. [CrossRef]

37. Nurhadi, M.; Widiyowati, I.I.; Wirhanuddin, W.; Chandren, S. Kinetic of Adsorption Process of Sulfonated Carbon-Derived from *Eichhornia crassipes* in the Adsorption of Methylene Blue Dye from Aqueous Solution. *Bull. Chem. React. Eng. Catal.* **2019**, *14*, 17–27. [CrossRef]

38. El Nemr, A.; Aboughaly, R.M.; El Sikaily, A.; Masoud, M.S.; Ramadan, M.S.; Ragab, S. Microporous-Activated Carbons of Type I Adsorption Isotherm Derived from Sugarcane Bagasse Impregnated with Zinc Chloride. *Carbon Lett.* **2022**, *32*, 229–249. [CrossRef]

39. Riyanto, C.A.; Prabalaras, E. The Adsorption Kinetics and Isoterm of Activated Carbon from Water Hyacinth Leaves (*Eichhornia crassipes*) on Co(II). *J. Phys. Conf. Ser.* **2019**, *1307*, 012002. [CrossRef]

40. Brunauer, S.; Emmett, P.H.; Teller, E. Adsorption of Gases in Multimolecular Layers. *J. Am. Chem. Soc.* **1938**, *60*, 309–319. [CrossRef]

41. Lee, S.-Y.; Choi, H.-J. Efficient Adsorption of Methylene Blue from Aqueous Solution by Sulfuric Acid Activated Watermelone Rind (*Citrullus lanatus*). *Korean Soc. Ind. Eng. Chem.* **2021**, *32*, 348–356.

42. Silva, M.S.; Silva, L.S.; Ferreira, F.J.L.; Bezerra, R.D.S.; Marques, T.M.F.; Meneguin, A.B.; Barud, H.S.; Osajima, J.A.; Silva Filho, E.C. Study of Interactions between Organic Contaminants and a New Phosphated Biopolymer Derived from Cellulose. *Int. J. Biol. Macromol.* **2020**, *146*, 668–677. [CrossRef] [PubMed]

43. Bezerra, R.D.S.; Leal, R.C.; da Silva, M.S.; Morais, A.I.S.; Marques, T.H.C.; Osajima, J.A.; Meneguin, A.B.; da S. Barud, H.; da Silva Filho, E.C. Direct Modification of Microcrystalline Cellulose with Ethylenediamine for Use as Adsorbent for Removal Amitriptyline Drug from Environment. *Molecules* **2017**, *22*, 2039. [CrossRef]

44. Saini, K.; Sahoo, A.; Biswas, B.; Kumar, A.; Bhaskar, T. Preparation and Characterization of Lignin-Derived Hard Templated Carbon(s): Statistical Optimization and Methyl Orange Adsorption Isotherm Studies. *Bioresour. Technol.* **2021**, *342*, 125924. [CrossRef]

45. Alemu, A.; Kerie, E. Removal of Acid Yellow 17 Dye from Aqueous Solutions Using Activated Water Hyacinth (*Eichhornia crassipes*). *Water Pract. Technol.* **2022**, *17*, 1294–1304. [CrossRef]

46. Patil, S.R.; Sutar, S.S.; Jadhav, J.P. Sorption of Crystal Violet from Aqueous Solution Using Live Roots of *Eichhornia crassipes*: Kinetic, Isotherm, Phyto and Cyto-Genotoxicity Studies. *Environ. Technol. Innov.* **2020**, *18*, 100648. [CrossRef]

47. Lagergren, S. About the Theory of So-Called Adsorption of Soluble Substances. *K. Sven. Vetenskapsakad. Handl.* **1898**, *24*, 1–39.

48. Ho, Y.S.; McKay, G. Pseudo-Second Order Model for Sorption Processes. *Process Biochem.* **1999**, *34*, 451–465. [CrossRef]

49. Akdemir, M.; Isik, B.; Cakar, F.; Cankurtaran, O. Comparison of the Adsorption Efficiency of Cationic (Crystal Violet) and Anionic (Congo Red) Dyes on *Valeriana officinalis* Roots: Isotherms, Kinetics, Thermodynamic Studies, and Error Functions. *Mater. Chem. Phys.* **2022**, *291*, 126763. [CrossRef]

50. Ferreira, F.J.L.; Silva, L.S.; da Silva, M.S.; Osajima, J.A.; Meneguin, A.B.; Santangeli, S.H.; Barud, H.S.; Bezerra, R.D.S.; Silva-Filho, E.C. Understanding Kinetics and Thermodynamics of the Interactions between Amitriptyline or Eosin Yellow and Aminosilane-Modified Cellulose. *Carbohydr. Polym.* **2019**, *225*, 115246. [CrossRef]

51. Bhat, A.H.; Chishti, H.-T.-N. Adsorption of Rhodamine-B by Polypyrrole Sn (IV) Tungstophosphate Nanocomposite Cation Exchanger: Kinetic-Cum-Thermodynamic Investigations. *Sep. Sci. Technol.* **2023**, *58*, 287–301. [CrossRef]

52. Liu, L.; Hu, S.; Shen, G.; Farooq, U.; Zhang, W.; Lin, S.; Lin, K. Adsorption Dynamics and Mechanism of Aqueous Sulfachloropy-ridazine and Analogues Using the Root Powder of Recyclable Long-Root *Eichhornia crassipes*. *Chemosphere* **2018**, *196*, 409–417. [CrossRef]

53. Amalina, F.; Razak, A.S.A.; Krishnan, S.; Zularisam, A.W.; Nasrullah, M. Water Hyacinth (*Eichhornia crassipes*) for Organic Contaminants Removal in Water—A Review. *J. Hazard. Mater. Adv.* **2022**, *7*, 100092. [CrossRef]

54. Freundlich, H. Über Die Adsorption in Lösungen. *Z. Phys. Chem.* **1907**, *57*, 385–470. [CrossRef]

55. Langmuir, D.; Herman, J.S. The Mobility of Thorium in Natural Waters at Low Temperatures. *Geochim. Cosmochim. Acta* **1980**, *44*, 1753–1766. [CrossRef]

56. Ma, Y. Comparison of Activated Carbons Prepared from Wheat Straw via ZnCl2 and KOH Activation. *Waste Biomass Valorization* **2017**, *8*, 549–559. [CrossRef]

57. Wang, Y.; Wang, S.; Xie, T.; Cao, J. Activated Carbon Derived from Waste Tangerine Seed for the High-Performance Adsorption of Carbamate Pesticides from Water and Plant. *Bioresour. Technol.* **2020**, *316*, 123929. [CrossRef] [PubMed]

58. Qi, X.; Huang, K.; Wu, X.; Zhao, W.; Wang, H.; Zhuang, Q.; Ju, Z. Novel Fabrication of N-Doped Hierarchically Porous Carbon with Exceptional Potassium Storage Properties. *Carbon* **2018**, *131*, 79–85. [CrossRef]

59. de Souza, C.C.; de Souza, L.Z.M.; Yılmaz, M.; de Oliveira, M.A.; da Silva Bezerra, A.C.; da Silva, E.F.; Dumont, M.R.; Machado, A.R.T. Activated Carbon of Coriandrum Sativum for Adsorption of Methylene Blue: Equilibrium and Kinetic Modeling. *Clean. Mater.* **2022**, *3*, 100052. [CrossRef]

60. Luo, X.; Cai, Y.; Liu, L.; Zeng, J. Cr(VI) Adsorption Performance and Mechanism of an Effective Activated Carbon Prepared from Bagasse with a One-Step Pyrolysis and ZnCl$_2$ Activation Method. *Cellulose* **2019**, *26*, 4921–4934. [CrossRef]

61. Cao, F.; Lian, C.; Yu, J.; Yang, H.; Lin, S. Study on the Adsorption Performance and Competitive Mechanism for Heavy Metal Contaminants Removal Using Novel Multi-Pore Activated Carbons Derived from Recyclable Long-Root *Eichhornia crassipes*. *Bioresour. Technol.* **2019**, *276*, 211–218. [CrossRef] [PubMed]

62. Samiyammal, P.; Kokila, A.; Pragasan, L.A.; Rajagopal, R.; Sathya, R.; Ragupathy, S.; Krishnakumar, M.; Minnam Reddy, V.R. Adsorption of Brilliant Green Dye onto Activated Carbon Prepared from Cashew Nut Shell by KOH Activation: Studies on Equilibrium Isotherm. *Environ. Res.* **2022**, *212*, 113497. [CrossRef] [PubMed]

63. Doan, V.D.; Tran, T.K.N.; Nguyen, A.-T.; Tran, V.A.; Nguyen, T.D.; Le, V.T. Comparative Study on Adsorption of Cationic and Anionic Dyes by Nanomagnetite Supported on Biochar Derived from *Eichhornia crassipes* and Phragmites Australis Stems. *Environ. Nanotechnol. Monit. Manag.* **2021**, *16*, 100569. [CrossRef]

64. Chen, S.; Qin, C.; Wang, T.; Chen, F.; Li, X.; Hou, H.; Zhou, M. Study on the Adsorption of Dyestuffs with Different Properties by Sludge-Rice Husk Biochar: Adsorption Capacity, Isotherm, Kinetic, Thermodynamics and Mechanism. *J. Mol. Liq.* **2019**, *285*, 62–74. [CrossRef]

65. Nasrullah, A.; Saad, B.; Bhat, A.H.; Khan, A.S.; Danish, M.; Isa, M.H.; Naeem, A. Mangosteen Peel Waste as a Sustainable Precursor for High Surface Area Mesoporous Activated Carbon: Characterization and Application for Methylene Blue Removal. *J. Clean. Prod.* **2019**, *211*, 1190–1200. [CrossRef]

66. Zhou, R.; Zhang, M.; Zhou, J.; Wang, J. Optimization of Biochar Preparation from the Stem of *Eichhornia crassipes* Using Response Surface Methodology on Adsorption of Cd^{2+}. *Sci. Rep.* **2019**, *9*, 17538. [CrossRef]

67. Boniolo, M.R.; Yabuki, L.N.M.; Mortari, D.A.; Menegário, A.A.; Garcia, M.L. Biomassas Brasileiras Aplicadas à Remoção de Urânio de Drenagem Ácida de Minas Por Processos de Biossorção. *Holos Environ.* **2017**, *17*, 149. [CrossRef]

68. Sulaiman, N.S.; Mohamad Amini, M.H.; Danish, M.; Sulaiman, O.; Hashim, R.; Demirel, S.; Demirel, G.K. Characterization and Ofloxacin Adsorption Studies of Chemically Modified Activated Carbon from Cassava Stem. *Materials* **2022**, *15*, 5117. [CrossRef]

69. Jaramillo-Martínez, D.; Buitrago-Sierra, R.; López, D. Use of Palm Oil Waste for Activated Carbons Production and Its Application in Methylene Blue Removal. *ChemistrySelect* **2022**, *7*, e202200791. [CrossRef]

70. Carneiro, M.T.; Barros, A.Z.B.; Morais, A.I.S.; Carvalho Melo, A.L.F.; Bezerra, R.D.S.; Osajima, J.A.; Silva-Filho, E.C. Application of Water Hyacinth Biomass (*Eichhornia crassipes*) as an Adsorbent for Methylene Blue Dye from Aqueous Medium: Kinetic and Isothermal Study. *Polymers* **2022**, *14*, 2732. [CrossRef]

71. Marques, T.M.F.; Sales, D.A.; Silva, L.S.; Bezerra, R.D.S.; Silva, M.S.; Osajima, J.A.; Ferreira, O.P.; Ghosh, A.; Silva Filho, E.C.; Viana, B.C.; et al. Amino-Functionalized Titanate Nanotubes for Highly Efficient Removal of Anionic Dye from Aqueous Solution. *Appl. Surf. Sci.* **2020**, *512*, 145659. [CrossRef]

72. Mbarki, F.; Selmi, T.; Kesraoui, A.; Seffen, M. Low-Cost Activated Carbon Preparation from Corn Stigmata Fibers Chemically Activated Using H_3PO_4, $ZnCl_2$ and KOH: Study of Methylene Blue Adsorption, Stochastic Isotherm and Fractal Kinetic. *Ind. Crops Prod.* **2022**, *178*, 114546. [CrossRef]

73. Singh, S.; Prajapati, A.K.; Chakraborty, J.P.; Mondal, M.K. Adsorption Potential of Biochar Obtained from Pyrolysis of Raw and Torrefied Acacia Nilotica towards Removal of Methylene Blue Dye from Synthetic Wastewater. *Biomass Convers. Biorefin.* **2023**, *13*, 6083–6104. [CrossRef]

74. Abbaci, F.; Nait-Merzoug, A.; Guellati, O.; Harat, A.; El Haskouri, J.; Delhalle, J.; Mekhalif, Z.; Guerioune, M. Bio/KOH Ratio Effect on Activated Biochar and Their Dye Based Wastewater Depollution. *J. Anal. Appl. Pyrolysis* **2022**, *162*, 105452. [CrossRef]

75. Subratti, A.; Vidal, J.L.; Lalgee, L.J.; Kerton, F.M.; Jalsa, N.K. Preparation and Characterization of Biochar Derived from the Fruit Seed of Cedrela Odorata L and Evaluation of Its Adsorption Capacity with Methylene Blue. *Sustain. Chem. Pharm.* **2021**, *21*, 100421. [CrossRef]

76. Sahu, S.; Pahi, S.; Tripathy, S.; Singh, S.K.; Behera, A.; Sahu, U.K.; Patel, R.K. Adsorption of Methylene Blue on Chemically Modified Lychee Seed Biochar: Dynamic, Equilibrium, and Thermodynamic Study. *J. Mol. Liq.* **2020**, *315*, 113743. [CrossRef]

77. Kar, S.; Santra, B.; Kumar, S.; Ghosh, S.; Majumdar, S. Sustainable Conversion of Textile Industry Cotton Waste into P-Dopped Biochar for Removal of Dyes from Textile Effluent and Valorisation of Spent Biochar into Soil Conditioner towards Circular Economy. *Environ. Pollut.* **2022**, *312*, 120056. [CrossRef]

78. Ying, Z.; Chen, X.; Li, H.; Liu, X.; Zhang, C.; Zhang, J.; Yi, G. Efficient Adsorption of Methylene Blue by Porous Biochar Derived from Soybean Dreg Using a One-Pot Synthesis Method. *Molecules* **2021**, *26*, 661. [CrossRef]

79. Ma, Y.; Zheng, D.; Mo, Z.; Dong, R.; Qiu, X. Magnetic Lignin-Based Carbon Nanoparticles and the Adsorption for Removal of Methyl Orange. *Colloids Surf. A Physicochem. Eng. Asp.* **2018**, *559*, 226–234. [CrossRef]

80. Chen, Y.; Liu, J.; Zeng, Q.; Liang, Z.; Ye, X.; Lv, Y.; Liu, M. Preparation of Eucommia Ulmoides Lignin-Based High-Performance Biochar Containing Sulfonic Group: Synergistic Pyrolysis Mechanism and Tetracycline Hydrochloride Adsorption. *Bioresour. Technol.* **2021**, *329*, 124856. [CrossRef]

81. Raj, A.; Yadav, A.; Rawat, A.P.; Singh, A.K.; Kumar, S.; Pandey, A.K.; Sirohi, R.; Pandey, A. Kinetic and Thermodynamic Investigations of Sewage Sludge Biochar in Removal of Remazol Brilliant Blue R Dye from Aqueous Solution and Evaluation of Residual Dyes Cytotoxicity. *Environ. Technol. Innov.* **2021**, *23*, 101556. [CrossRef]

82. Islam, M.A.; Benhouria, A.; Asif, M.; Hameed, B.H. Methylene Blue Adsorption on Factory-Rejected Tea Activated Carbon Prepared by Conjunction of Hydrothermal Carbonization and Sodium Hydroxide Activation Processes. *J. Taiwan Inst. Chem. Eng.* **2015**, *52*, 57–64. [CrossRef]

83. Rawat, A.P.; Singh, D.P. Decolourization of Malachite Green Dye by Mentha Plant Biochar (MPB): A Combined Action of Adsorption and Electrochemical Reduction Processes. *Water Sci. Technol.* **2018**, *77*, 1734–1743. [CrossRef] [PubMed]

84. Oraon, A.; Prajapati, A.K.; Ram, M.; Saxena, V.K.; Dutta, S.; Gupta, A.K. Synthesis, Characterization, and Application of Microporous Biochar Prepared from *Pterospermum acerifolium* Plant Fruit Shell Waste for Methylene Blue Dye Adsorption: The Role of Surface Modification by SDS Surfactant. *Biomass Convers. Biorefin.* **2022**, 1–23. [CrossRef]

85. Cuong Nguyen, X.; Thanh Huyen Nguyen, T.; Hong Chuong Nguyen, T.; Van Le, Q.; Yen Binh Vo, T.; Cuc Phuong Tran, T.; Duong La, D.; Kumar, G.; Khanh Nguyen, V.; Chang, S.W.; et al. Sustainable Carbonaceous Biochar Adsorbents Derived from Agro-Wastes and Invasive Plants for Cation Dye Adsorption from Water. *Chemosphere* **2021**, *282*, 131009. [CrossRef]

86. Fu, H.; Ma, S.; Zhao, P.; Xu, S.; Zhan, S. Activation of Peroxymonosulfate by Graphitized Hierarchical Porous Biochar and MnFe2O4 Magnetic Nanoarchitecture for Organic Pollutants Degradation: Structure Dependence and Mechanism. *Chem. Eng. J.* **2019**, *360*, 157–170. [CrossRef]

87. Pandey, D.; Daverey, A.; Dutta, K.; Yata, V.K.; Arunachalam, K. Valorization of Waste Pine Needle Biomass into Biosorbents for the Removal of Methylene Blue Dye from Water: Kinetics, Equilibrium and Thermodynamics Study. *Environ. Technol. Innov.* **2022**, *25*, 102200. [CrossRef]

88. Zhou, J.; Jiang, Z.; Qin, X.; Zhang, L.; Huang, Q.; Xu, G. Effects and Mechanisms of Calcium Ion Addition on Lead Removal from Water by *Eichhornia crassipes*. *Int. J. Environ. Res. Public. Health* **2020**, *17*, 928. [CrossRef]

89. Chen, Y.-P.; Zheng, C.-H.; Huang, Y.-Y.; Chen, Y.-R. Removal of Chlortetracycline from Water Using Spent Tea Leaves-Based Biochar as Adsorption-Enhanced Persulfate Activator. *Chemosphere* **2022**, *286*, 131770. [CrossRef]

90. Extross, A.; Waknis, A.; Tagad, C.; Gedam, V.V.; Pathak, P.D. Adsorption of Congo Red Using Carbon from Leaves and Stem of Water Hyacinth: Equilibrium, Kinetics, Thermodynamic Studies. *Int. J. Environ. Sci. Technol.* **2023**, *20*, 1607–1644. [CrossRef]

91. Jabar, J.M.; Odusote, Y.A.; Ayinde, Y.T.; Yılmaz, M. African Almond (*Terminalia catappa* L.) Leaves Biochar Prepared through Pyrolysis Using H_3PO_4 as Chemical Activator for Sequestration of Methylene Blue Dye. *Results Eng.* **2022**, *14*, 100385. [CrossRef]

92. Nworie, F.S.; Nwabue, F.I.; Oti, W.; Mbam, E.; Nwali, B.U. Removal of methylene blue from aqueous solution using activated rice husk biochar: Adsorption isotherms, kinetics and error analysis. *J. Chil. Chem. Soc.* **2019**, *64*, 4365–4376. [CrossRef]

93. Viswanthan, S.P.; Neelamury, S.P.; Parakkuzhiyil, S.; Njazhakunnathu, G.V.; Sebastian, A.; Padmakumar, B.; Ambatt, T.P. Removal Efficiency of Methylene Blue from Aqueous Medium Using Biochar Derived from Phragmites Karka, a Highly Invasive Wetland Weed. *Biomass Convers. Biorefin.* **2022**, *12*, 3257–3273. [CrossRef]

94. Widiyowati, I.I.; Nurhadi, M.; Hatami, M.; Yuan, L.S. Effective TiO_2-Sulfonated Carbon-Derived from *Eichhornia crassipes* in The Removal of Methylene Blue and Congo Red Dyes from Aqueous Solution. *Bull. Chem. React. Eng. Catal.* **2020**, *15*, 476–489. [CrossRef]

95. Rahman, M.W.; Nipa, S.T.; Rima, S.Z.; Hasan, M.M.; Saha, R.; Halim, M.A.; Ali, Y.; Deb, A. Pseudo-Stem Banana Fiber as a Potential Low-Cost Adsorbent to Remove Methylene Blue from Synthetic Wastewater. *Appl. Water Sci.* **2022**, *12*, 242. [CrossRef]

96. Lakkaboyana, S.K.; Khantong, S.; Asmel, N.K.; Yuzir, A.; Wan Yaacob, W.Z. Synthesis of Copper Oxide Nanowires-Activated Carbon (AC@CuO-NWs) and Applied for Removal Methylene Blue from Aqueous Solution: Kinetics, Isotherms, and Thermodynamics. *J. Inorg. Organomet. Polym. Mater.* **2019**, *29*, 1658–1668. [CrossRef]

97. Li, H.; Liu, L.; Cui, J.; Cui, J.; Wang, F.; Zhang, F. High-Efficiency Adsorption and Regeneration of Methylene Blue and Aniline onto Activated Carbon from Waste Edible Fungus Residue and Its Possible Mechanism. *RSC Adv.* **2020**, *10*, 14262–14273. [CrossRef] [PubMed]

98. Abdel-Aziz, M.H.; El-Ashtoukhy, E.Z.; Bassyouni, M.; Al-Hossainy, A.F.; Fawzy, E.M.; Abdel-Hamid, S.M.S.; Zoromba, M.S. DFT and Experimental Study on Adsorption of Dyes on Activated Carbon Prepared from Apple Leaves. *Carbon. Lett.* **2021**, *31*, 863–878. [CrossRef]

99. Fito, J.; Abrham, S.; Angassa, K. Adsorption of Methylene Blue from Textile Industrial Wastewater onto Activated Carbon of Parthenium Hysterophorus. *Int. J. Environ. Res.* **2020**, *14*, 501–511. [CrossRef]

100. Hakami, O. Biochar-Derived Activated Carbons: A Comprehensive Assessment of Kinetic and Isotherm Modeling for Adsorptive Removal of Methylene Blue Dye Contaminants. *Int. J. Environ. Sci. Technol.* **2023**, *20*, 10325–10344. [CrossRef]

101. Achour, Y.; Bahsis, L.; Ablouh, E.-H.; Yazid, H.; Laamari, M.R.; Haddad, M. El Insight into Adsorption Mechanism of Congo Red Dye onto Bombax Buonopozense Bark Activated-Carbon Using Central Composite Design and DFT Studies. *Surf. Interfaces* **2021**, *23*, 100977. [CrossRef]

102. Tejada-Tovar, C.; Paz, I.; Acevedo-Correa, D.; Espinosa-Fortich, M.; López-Badel, C. Adsorption of Chrome (VI) and Mercury (II) in Solution Using Hyacinth (*Eichhornia crassipes*). *Biotecnol. Sect. Agropecu. Agroind.* **2021**, *19*, 54–65. [CrossRef]

103. Sharma, S.; Sharma, G.; Kumar, A.; AlGarni, T.S.; Naushad, M.; ALOthman, Z.A.; Stadler, F.J. Adsorption of Cationic Dyes onto Carrageenan and Itaconic Acid-Based Superabsorbent Hydrogel: Synthesis, Characterization and Isotherm Analysis. *J. Hazard. Mater.* **2022**, *421*, 126729. [CrossRef]

104. Tran, H.N.; Lima, E.C.; Juang, R.-S.; Bollinger, J.-C.; Chao, H.-P. Thermodynamic Parameters of Liquid–Phase Adsorption Process Calculated from Different Equilibrium Constants Related to Adsorption Isotherms: A Comparison Study. *J. Environ. Chem. Eng.* **2021**, *9*, 106674. [CrossRef]

105. Gao, F.; Xu, X.; Yang, J. Removal of *p*-Nitrophenol from Simulated Sewage Using MgCo-3D Hydrotalcite Nanospheres: Capability and Mechanism. *RSC Adv.* **2022**, *12*, 27044–27054. [CrossRef]

106. Shoaib, A.G.M.; El Sikaily, A.; Ragab, S.; Masoud, M.S.; Ramadan, M.S.; El Nemr, A. Starch-Grafted-Poly(Acrylic Acid)/Pterocladia Capillacea–Derived Activated Carbon Composite for Removal of Methylene Blue Dye from Water. *Biomass Convers. Biorefin.* **2022**, 1–21. [CrossRef]

107. Durrani, W.Z.; Nasrullah, A.; Khan, A.S.; Fagieh, T.M.; Bakhsh, E.M.; Akhtar, K.; Khan, S.B.; Din, I.U.; Khan, M.A.; Bokhari, A. Adsorption Efficiency of Date Palm Based Activated Carbon-Alginate Membrane for Methylene Blue. *Chemosphere* **2022**, *302*, 134793. [CrossRef]

108. Trung Hiep, N.; Thi Hoai Thu, T.; Thi Thanh Quyen, L.; Dinh Dong, P.; Tuyet Suong, T.; Phuong Vu, T. Biochar Derived from Sesbania Sesban Plant as a Potential Low-Cost Adsorbent for Removal of Methylene Blue. *Environ. Nat. Resour. J.* **2022**, *20*, 611–620. [CrossRef]

109. Sulaiman, N.S.; Mohamad Amini, M.H.; Danish, M.; Sulaiman, O.; Hashim, R. Kinetics, Thermodynamics, and Isotherms of Methylene Blue Adsorption Study onto Cassava Stem Activated Carbon. *Water* **2021**, *13*, 2936. [CrossRef]

110. Buvaneswari, K.; Singanan, M. Removal of Malachite Green Dye in Synthetic Wastewater Using Zingiber Officinale Plant Leaves Biocarbon. *Mater. Today Proc.* **2022**, *55*, 274–279. [CrossRef]

111. Patil, S.A.; Kumbhar, P.D.; Satvekar, B.S.; Harale, N.S.; Bhise, S.C.; Patil, S.K.; Sartape, A.S.; Kolekar, S.S.; Anuse, M.A. Adsorption of Toxic Crystal Violet Dye from Aqueous Solution by Using Waste Sugarcane Leaf-Based Activated Carbon: Isotherm, Kinetic and Thermodynamic Study. *J. Iran. Chem. Soc.* **2022**, *19*, 2891–2906. [CrossRef]

112. Jawad, A.H.; Surip, S.N. Upgrading Low Rank Coal into Mesoporous Activated Carbon via Microwave Process for Methylene Blue Dye Adsorption: Box Behnken Design and Mechanism Study. *Diam. Relat. Mater.* **2022**, *127*, 109199. [CrossRef]

113. Singh, V.; Srivastava, V.C. Self-Engineered Iron Oxide Nanoparticle Incorporated on Mesoporous Biochar Derived from Textile Mill Sludge for the Removal of an Emerging Pharmaceutical Pollutant. *Environ. Pollut.* **2020**, *259*, 113822. [CrossRef]

114. Farooq, S.; Al Maani, A.H.; Naureen, Z.; Hussain, J.; Siddiqa, A.; Al Harrasi, A. Synthesis and Characterization of Copper Oxide-Loaded Activated Carbon Nanocomposite: Adsorption of Methylene Blue, Kinetic, Isotherm, and Thermodynamic Study. *J. Water Process Eng.* **2022**, *47*, 102692. [CrossRef]

115. Yadav, S.K.; Dhakate, S.R.; Pratap Singh, B. Carbon Nanotube Incorporated Eucalyptus Derived Activated Carbon-Based Novel Adsorbent for Efficient Removal of Methylene Blue and Eosin Yellow Dyes. *Bioresour. Technol.* **2022**, *344*, 126231. [CrossRef] [PubMed]

116. Belcaid, A.; Beakou, B.H.; Bouhsina, S.; Anouar, A. Insight into Adsorptive Removal of Methylene Blue, Malachite Green, and Rhodamine B Dyes by Cassava Peel Biochar (*Manihot esculenta* Crantz) in Single, Binary, and Ternary Systems: Competitive Adsorption Study and Theoretical Calculations. *Biomass Convers. Biorefin.* **2022**, 1–24. [CrossRef]

117. Roy, S.; Mondal, D.K. Parametric Optimization and Kinetics Study of Effective Removal of Methylene Blue by Citric Acid-Modified Arjun Bark Powder. *Biomass Convers. Biorefin.* **2022**, 1–12. [CrossRef]

118. Pandey, D.; Daverey, A.; Dutta, K.; Arunachalam, K. Enhanced Adsorption of Congo Red Dye onto Polyethyleneimine-Impregnated Biochar Derived from Pine Needles. *Environ. Monit. Assess.* **2022**, *194*, 880. [CrossRef]

119. Hien Tran, T.; Le, A.H.; Pham, T.H.; Duong, L.D.; Nguyen, X.C.; Nadda, A.K.; Chang, S.W.; Chung, W.J.; Nguyen, D.D.; Nguyen, D.T. A Sustainable, Low-Cost Carbonaceous Hydrochar Adsorbent for Methylene Blue Adsorption Derived from Corncobs. *Environ. Res.* **2022**, *212*, 113178. [CrossRef]

120. Shah, S.S.; Sharma, T.; Kumar, D.; Sharma, S.; Bamezai, R.K. Ionic Liquid Treated Leaves of *Juglans regia* as an Adsorbent for the Removal of Methyl Orange Dye: Experimental, Computational, and Statistical Approach. *Int. J. Phytoremediat.* **2023**, *25*, 765–780. [CrossRef]